UNIVERSITÀ DEGLI STUDI DI PADOVA

Facoltà di Scienze MM.NN.FF.
Facoltà di Ingegneria

ISTITUTO NAZIONALE DI FISICA NUCLEARE

Laboratori Nazionali di Legnaro

in collaboration with Confindustria Veneto

MASTER THESIS

in

"Surface Treatments for Industrial Applications"

Magnetron sputtering of Superconducting Multilayer Nb_3Sn Thin Film

Supervisor: Prof. V. Palmieri

Co-Supervisor: Dr. A.A.Rossi

Student: Jinhai Li

Matr. N°: 938770

Academic Year 2009-10

A Poem Inscribed on the Wall of a Monastery

Song Dynasty ● Su Shi

Regard the mountains as a range from the front and peaks from the side;

The mountain looks different when changing your viewpoint from afar or near, from up or down;

One cannot recognize the true appearance of Lushan Mount;

It is just because that you are in the mountains.

题西林壁

宋 ● 苏轼

横看成岭侧成峰，

远近高低各不同，

不识庐山真面目，

只缘身在此山中。

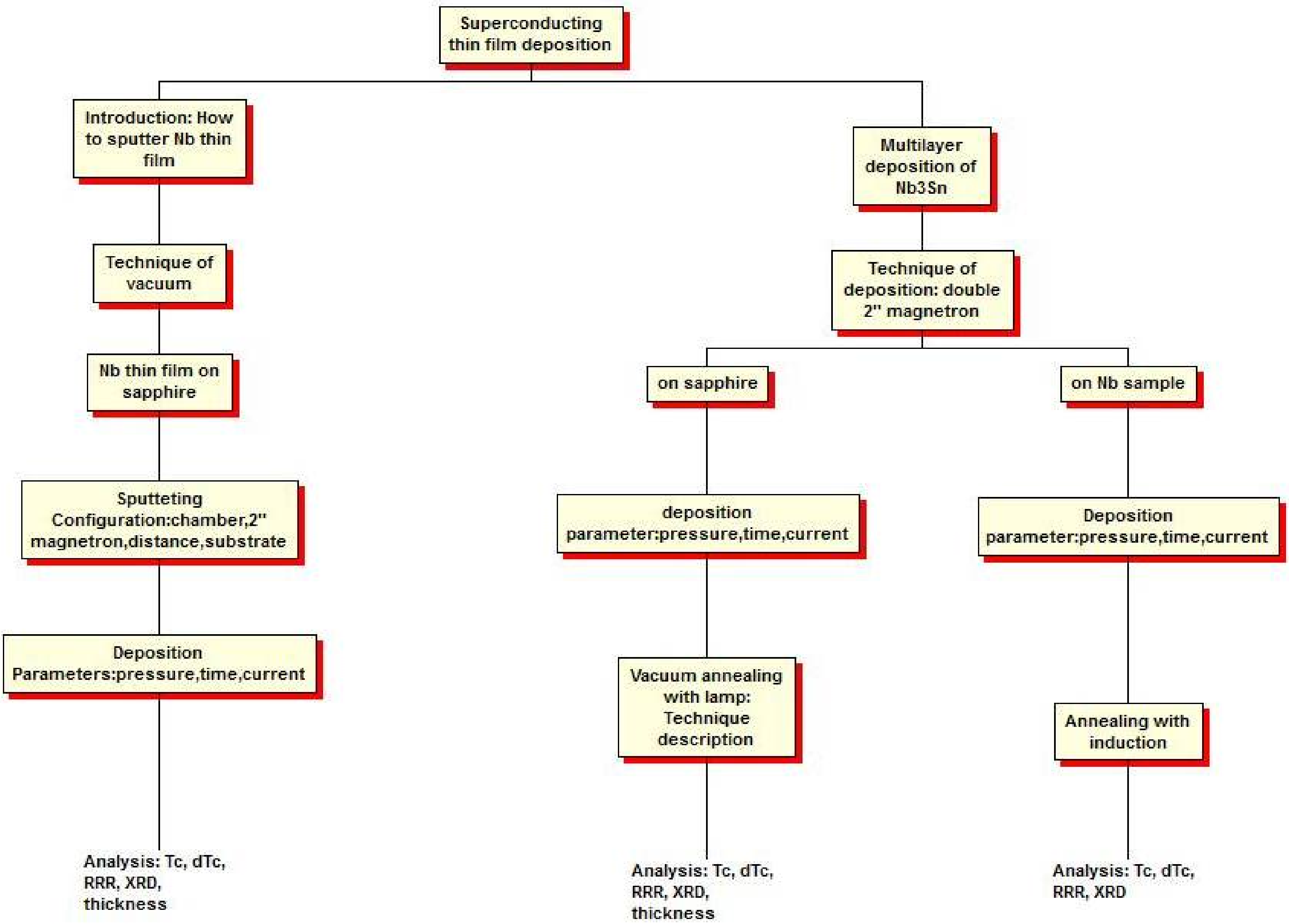
Superconducting thin film deposition
Introduction: How to sputter Nb thin film
Technique of vacuum
Nb thin film on sapphire
Sputteting Configuration:chamber,2" magnetron,distance,substrate
Deposition Parameters:pressure,time,current
Analysis: Tc, dTc, RRR, XRD, thickness
Multilayer deposition of Nb3Sn
Technique of deposition: double 2" magnetron
on sapphire
deposition parameter:pressure,time,current
Vacuum annealing with lamp: Technique description
Analysis: Tc, dTc, RRR, XRD, thickness
on Nb sample
Deposition parameter:pressure,time,current
Annealing with induction
Analysis: Tc, dTc, RRR, XRD

Index

INDEX ..... **VII**

INTRODUCTION **1**

CHAPTER 1 AN INTRODUCTION OF SUPERCONDUCTOR CAVITY **2**

1.1 THE NECESSARY OF SUPERCONDUCTOR RF ACCELERATOR 2
1.2 THE PERFORMANCE OF THE NEEDED SUPERCONDUCTOR CAVITY 4
1.3 THE NECESSARY OF NB_3SN SUPERCONDUCTOR THIN FILM 7

CHAPTER 2 INTRODUCTION: HOW TO SPUTTER NB THIN FILM **20**

2.1 TECHNIQUE OF THE VACUUM 20
2.2 NB THIN FILM ON SAPPHIRE 26
2.2.1 Sputtering configuration *26*
2.2.2 Deposition parameter *29*
2.2.3 Analysis and results *30*
2.2.3.1 Thickness measurement 30
2.2.3.2 Tc measurement 31
2.2.3.3 XRD analysis 35
2.3 DISCUSSION 40

CHAPTER 3 MULTILAYER DEPOSITION OF NB_3SN **41**

3.1 TECHNIQUE OF DEPOSITION 41
3.2 DEPOSITION ON SAPPHIRE 42
3.2.1 Deposition parameter *42*
3.2.2 Vacuum annealing *43*
3.2.2.1 The technique description of lamp annealing 44
3.2.2.2 Analysis result 47
3.3 DEPOSITION ON NB SAMPLE 54
3.3.1 Deposition parameter *56*
3.3.2 Annealing with inductor *56*
3.3.3 Analysis result *59*
3.3.3.1 Tc measurement 59
3.3.3.2 XRD analysis 65
3.4 CONCLUSION 72

Introduction

The superconductor accelerator cavity is one of the most important and perspective technology for an advance accelerator. For example, the International Committee for Future Accelerators decided that the Linear Collider design had been based on the superconductor technology. Moreover, the accelerator operating with continue wave (CW) mode must use the superconductor technology in stead of the normal conductor technology, such as the Accelerator-driven sub-critical reactor system (ADS), the Accelerator Transmutation of Waste (ATW), the Accelerator Production of Tritium (APT), and so on.

In order to meet all kinds of application, the scientific world interest is now focus on further developments of new resonant cavities fabrication techniques to reduce cost and improve the performance of the accelerator cavity. To realize this object, one of the important methods is to pursue research on new materials. The goal will be the achievement of superconducting cavity working better the Nb ones at 4.2K. For example, the better parameters of the T_c, the surface resistance, the critical field H_c and the Q value are needed.

Up to now, the most possible candidate is Nb_3Sn. The Nb_3Sn has not only the better superconductivity parameters, but also the stable property and the easy fabrication. There are two methods to fabricate the superconductor cavity with the Nb_3Sn, which are including the diffusion method and the multilayer deposition method. In the thesis, we focus on the multilayer deposition method, and the content of each chapter is followed:

In chapter 1, we discuss why we select the Nb_3Sn as the function material for the superconductor cavity fabrication.

In chapter 2, we first investigate the Nb thin film deposition on the sapphire, and analysis the result of the deposition experiment.

In chapter 3, the Nb_3Sn multilayer thin film is first deposited on the sapphire, and then deposited on the Nb sample. The deposition experiment results are also analyzed with T_c and crystal structure.

The outline of this thesis is shown as follow:

Chapter 1 An Introduction of superconductor cavity

1.1 The necessary of superconductor RF accelerator

The particle accelerator is a very important instrument. It can be used in the industry, agriculture, hospital, energy sources, science, and so on. It is first used for the science and the most advanced accelerator is still used for.

In the industry, the accelerator is used for ion implantation for semiconductor, surface modification and so on. In the hospital, the accelerator is used for radiation therapy, radioactive isotope production, and so on. In the energy sources field, the accelerator is used in the Accelerator-driven sub-critical reactor system (ADS), the Accelerator Transmutation of Waste (ATW), the Accelerator Production of Tritium (APT), and so on. The ADS means that a sub-critical reactor driven by the neutron can produce energy. The neutron is first produced by target injected with the proton beam accelerated by an accelerator, and can be controlled by the amount of the proton injected. Because the reactor is sub-critical, it is more safe than the traditional. The ATW and the APT have some similar with the ADS that they all produce the neutron by the proton beam of the accelerator first. The ATW use the neutron to transmute the high radioactive waste produced by the reactor into low radioactive waste. The APT uses the reaction between the neutron and the Helium-3 to produce the Tritium.

In the science field, the scientist has infinite interest in the mysterious universe. From 400 years ago, Galileo used the telescope to research the macro-universe. Up to now, we use the Hubble and the LIGO. In the other side, the scientist has the great interest in the micro-universe. The scientist used the microscope to research the micro-universe also from about 400 years ago. Only form about 90 years ago, the scientist invented the particle accelerator and can deep the research field to the atom. After that, the particle accelerator was developed very quickly to obtain the higher and higher energy of the particle. Up to now, the LHC which can accelerate the proton up to 7 TeV had been built.

At the beginning, the particle was accelerated by the electrostatic field. The particle energy is from several KeV to several MeV. But there is a limitation of the energy of the particle accelerated by the electrostatic field. It is impossible to obtain more than 20 MeV. However, the scientist invented the acceleration method by radio frequency (RF). After that, the accelerator energy grows rapidly.

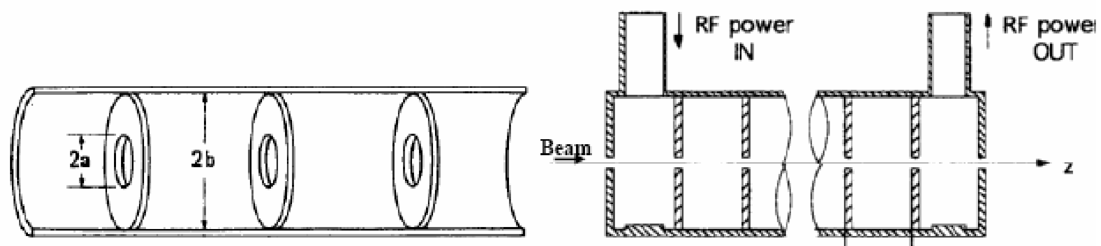

Fig. 1.1 Disc-loaded traveling-wave accelerator structure

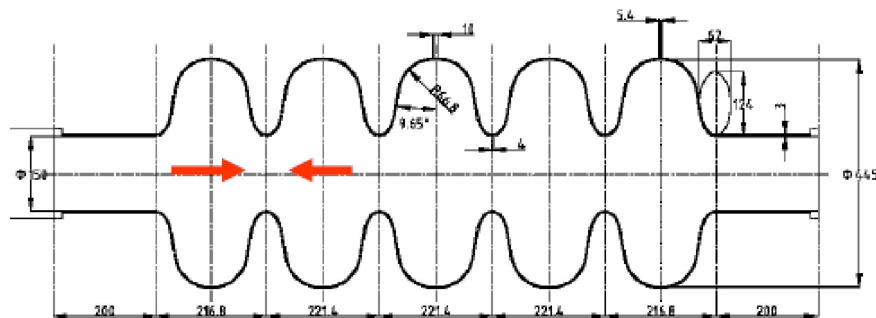

Fig. 1.2 standing-wave elliptic cavity accelerator structure

To accelerate the particle, the RF field should be confined in a cavity. For the electron beam, there are two kinds of accelerator structure which include standing wave structure and traveling wave structure. For the heavy ion beam, only the standing wave structure can be used, but there are many kinds of structure type, such as radio frequency quadruple (RFQ), drift tube linac (DTL), quarter wave resonators (QWR), half wave resonators (HWR), spoke resonator, elliptic cavity, and so on.

In the accelerator cavity, the energy of the RF field not only transfers to the particle, but also consumes on the wall of the cavity. For the high gradient normal conductor cavity, most of RF energy consumes on the wall. In order to improve the transfer efficient of the RF energy, the superconductor is taken into account. Almost all of the RF energy transfer to the particle by the superconductor cavity.

For the heavy ion, we can use a circular accelerator to obtain the high energy. In the circular accelerator, the particle can be accelerated many times by the same cavity when it runs along the circle in order to reduce the length of the accelerator and the number of the accelerator cavity. However, for the electron when its energy is higher than 200GeV, it can not be accelerated in the circular accelerator, because the electron will emit synchrotron photon and loss lots of energy when it bends in the circular accelerator. In consequence, the cost of circular accelerator is higher than that of the linear accelerator. So, only the linear accelerator is suitable for obtaining the energy of

electron higher than 200GeV.

The linear accelerators utilize a linear array of RF cavities and become increasingly long, with lengths up to the tens of kilometer range, to achieve particle energies in the GeV to TeV energy range that is of present High Energy Physics (HEP) interest. Such systems will require on the order of 20,000 RF cavities. Improving the accelerating voltage per unit length will result in tremendous cost savings, since the required length to achieve a given beam energy in a linear accelerator is inversely proportional to the electric field that can be generated per unit length. In addition, power requirements are significant, ranging from 100 to 250 MW for a 500 GeV linear accelerator.

The main figures of merit for RF cavities are the quality factor Q_0 (defined by the ratio between the energy stored in the cavity and the energy loss in one RF period) and its average accelerating field E_{acc}. Q_0 values as high as 10^{11} have been achieved in superconducting cavities. Superconducting cavities exhibit approximately a factor 10^6 higher Q_0 than normal conducting cavities due to the reduced microwave surface resistance. Even when accounting for cooling penalties the required input power is still about a factor 10^3 lower when using superconducting cavities instead of normal conducting cavities, saving drastically in operating costs. The International Technology Recommendation Panel of the International Committee for Future Accelerators therefore, amongst other considerations, selected superconducting RF cavities above normal conducting cavities as the preferred technology for future linear accelerators [1].

1.2 The performance of the needed superconductor cavity

The efficiency of a RF cavity is usually depicted by plotting Q_0 as a function of E_{acc}. For an ideal superconducting cavity, Q_0 remains constant with increasing E_{acc} and collapses when a maximum E_{acc} is reached. This point is determined by the magnetic components of the RF standing wave. Once the magnetic component reaches a certain threshold value, vortices penetrate the superconductor and the Meissner state is lost. Vortices that move inside the superconductor dissipate energy and cause the cavity to quench. Even though vortices can be elastically pinned by material imperfections, their oscillations in an RF field will still cause dissipations [2]. Hence, vortex penetration has to be prevented to retain a high Q_0 and a cavity has to operate in the Meissner state.

In Type-II superconductors, vortex penetration becomes energetically favorable at the bulk lower critical magnetic field H_{c1}. However, in magnetic fields which are parallel to the surface, vortices have to overcome the Bean-Livingston positive surface energy barrier to enter the superconductor [3]. The Meissner state can therefore persist metastably beyond H_{c1}, up to the so-called superheating field H_{sh}, at which the surface barrier disappears. Note that in practice H_{sh} is not necessarily reached, due to earlier vortex penetration at surface irregularities [4] and demagnetization effects of transverse magnetic field components [5].

So, one of the fundamental limitations of increasing the accelerating gradient of the superconductor cavity is the critical magnetic field H_{c1} of the RF field, which is also called as H^{rf}_{c} [6]. Other limitations include the electron field emission, the thermal breakdown, the surface resistance and T_c.

The electron field emission means that the electron emits from the peak of the cavity surface with high electrical field, which can decrease the Q value and induce local heat. The worst case of the electron field emission is the electrical breakdown. The electron field emission can be improved by optimizing the cavity shape to reduce the electrical field on the surface and improving the roughness of the surface.

The thermal breakdown is also a kind of local effect. If some particle without superconductivity adhere or embed in the surface, the heat will be produced when the electron pass through them. If the heat is high enough, it will heat the superconductivity atom near the particle to case the superconductivity, and then induce more atoms to case the superconductivity, at last, the whole cavity may case the superconductivity. One method to avoid the thermal breakdown is that the temperature of the superconductor cavity operating is great lower than T_c. The T_c is the critical temperature of superconductor. When the temperature of the conductor decreases lower than the T_c, the conductor changes from the normal state to the superconductivity state.

The resistance of the superconductor can be neglected at the condition of DC current. For the RF field, although the resistance of the superconductor is very small, it can not be neglected.

For the normal conductor, RF currents flow only on the surface of conductors without passing through the internal conductor bodies. The penetration depth of RF current in conductor is

$$\delta = \frac{1}{\sqrt{\pi f \mu \sigma}} \qquad (1.1)$$

Where, f is the frequency, μ is the permeability and σ is conductivity of the conductor.

In fact, after only a few penetration depths, in conductor internal body the RF current becomes negligible. The surface resistance of a conductor is

$$R_S^n = \frac{1}{\delta\sigma} = \sqrt{\frac{\pi f \mu}{\sigma}} \quad (1.2)$$

It is obvious that the penetration depth will increase and the surface resistance will decrease when the frequency decreases. At GHz range, only a few microns of the copper surface gives a contribution to the RF current, while the rest major part served as substrate.

The RF losses of the accelerator cavity, in the absence of vortices, are mainly determined by the RF surface resistance (R_S), which is usually represented as a summation of the Bardeen-Cooper-Schrieffer (BCS) surface resistance R_{BCS} and a residual resistance term (R_{res}) as shown in Eq.1.3. R_{res} is usually on the order of a few nΩ. Provided that the surface is clean and properly manufactured, R_S is usually dominated by R_{BCS}.

$$R_S = R_{ph} + R_{res} = R_{BCS} + R_{res} \quad (1.3)$$

Where, R_{ph} is the phonons resistance. The phonons resistance comes from the crystal lattice and is same with the BCS resistance. Among the factors that define the R_{res}, there are extrinsic causes e.g. trapped magnetic flux, can be avoided. Other causes are intrinsic and due to the structural imperfections of the material. Like inhomogeneities, impurities, grain boundaries or surface serrations. Materials with a large coherent length will be insensitive to large defects without an appreciable increase of the R_{res}. This is quite desirable for applications of the superconductor cavity, since the superconducting surfaces are exposed to RF field, and are difficult to prepare completely 'defect-free'. Therefore it is important to minimize the residual surface resistance. The R_{BCS} can be defined as:

$$R_{BCS} = \frac{A}{T}\sigma_n \omega^3 \lambda^2 e^{-\frac{BTc}{T}} \quad (1.4)$$

Where, A and B are two constants weakly depend on material, ω is the RF angular frequency, σ_n is the normal state conductivity of the material, λ is the effective penetration depth, and T_c is the critical temperature.

Because the surface resistance of superconductor in the RF field is non-zero, a tiny RF loss can heat the superconductor surface. So the more cryogenic power is

needed for preventing the superconductivity ceasing as shown in Table 1.1 [7]. In Table 1.1, Dynamic means to put the RF power into the superconductor cavity. At 2K, the ratio of the installed power over heat load is about 1000, but at 8K, the ratio is about 250. This means that the cryogenic power per unit of heat load at 2K is about four times of that at 8K. This conclusion also can be obtained by the Carnot cycle:

$$\frac{P_{cool}}{P_{source}} \geq \frac{T_2 - T_1}{T_1} \qquad (1.5)$$

Where, T_2 is the room temperature, T_1 is the cryogenic temperature. Because $T_2 >> T_1$, the ratio should be inverse proportion to T_1.

Table 1.1 RF unit cryogenic heat loads and installed AC cryogenic plant power to remove the heat.

	40–80 K		5–8 K		2 K		Total
	Static	Dynamic	Static	Dynamic	Static	Dynamic	
Heat load (W)	177.6	270.3	31.7	12.5	5.1	29.0	
Installed power (kW)	4.4	6.2	9.6	3.5	8.1	28.5	60.4

In order to decrease the cryogenic power, two parameters should be taken into account. The first parameter is the surface resistance, and the second is the cryogenic operation temperature. According to the Eq.(1.3), we should decrease R_{res} and R_{BCS}. To decrease R_{res}, we should increase the residual resistance radio (RRR).

$$RRR = \frac{R(300K)}{R_{res}} = 1 + \frac{R_{phonons}(300K)}{R_{res}} \qquad (1.6)$$

Where, $R_{phonons}(300K)$ is a constant.

According to the Eq.(1.4), to decrease R_{BCS}, we should increase the critical temperature T_c and decrease the cryogenic operation temperature T. However, according to the Eq.(1.5), to decrease the cryogenic power, we should increase the cryogenic operation temperature T. So, the best way is to increase T_c.

1.3 The necessary of Nb_3Sn superconductor thin film

Among the pure metal, Niobium have the highest T_c, which is about 9.2K. However, in order to obtain the better performances, such as Q value, accelerating gradients, thermal stability, and so on, the Nb cavity should only operate at the temperatures below 2.1 K, which is under the very expensive superfluid He bath cooling conditions. Fortunately, some of metal compounds have the Tc higher than

10K as shown in Table 1.2 and Table 1.3[8], and there is some possibility of operating at the temperature of 4.2K.

Table 1.2 Critical Temperature of compounds with B1 structure

B \ A	Sc	Y	La	Ti	Zr	Hf	V	Nb	Ta	Cr	Mo	W	Re
B					3.4	3.1							
C	<1.38	<1.38		3.42	<0.3	<1.20	0.03 3.2*	12	10.35		14.3	10.0	3.4
N	<1.38	<1.4	1.35	5.49	10.7	8.83	8.5	17.3	6.5	<1.28	5.0	<1.38	
P			<1.68										
Sb		<1.02	<1.02										
O				2.0			<0.3	1.39					
S	<0.33	1.9	0.87		3.3								
Se	<0.33	2.5	1.02										
Te		2.05	1.48										

* T_C = 3.2 K was registered in vanadium carbide after implantation of C^+ ions s

Table 1.3 Critical temperature of binaryA15 compounds

Nontransition elements	T_c (K)	Transition elements	T_c (K)
Ti_3Sb	6.5	Ti_3Ir	4.2
$Zr_{80}Sn_{20}$[a]	0.92	Ti_3Pt	0.5
Zr–Pb	0.76	Zr_3Au	0.9
$Zr_{\sim 3}Bi$[b]	3.4	$V_{29}Re_{71}$	8.4
V–Al[c]	14	$V_{50}Os_{50}$	5.7
V_3Ga	15.9	$V_{65}Rh_{35}$	≃1
V_3Si	17.0	$V_{63}Ir_{37}$	1.7
$V_{\sim 3}Ge$	6	$V_{\sim 3}Pd$	0.08
$V_{\sim 3}Ge$[c]	11	V_3Pt	3.7
$V_{\sim 79}Sn_{\sim 21}$	3.8	$V_{76}Au_{24}$	3
$V_{77}As_{23}$	0.2	$Nb_{75}Os_{25}$	1.0
$V_{76}Sb_{24}$	0.8	$Nb_{75}Rh_{25}$	2.6
Nb_3Al	19.1	$Nb_{72}Ir_{28}$	3.2
Nb_3Ga	20.7	Nb_3Pt	11
$Nb_{\sim 3}In$[b]	9.2	$Nb_{\sim 3}Au$	11.5
$Nb_{82}Si_{18}$[a]	4.4	$Ta_{85}Pt_{15}$	0.4
Nb–Si[c]	11–17	$Ta_{\sim 80}Au_{20}$	0.55
Nb–Ge[a]	17	$Cr_{72}Ru_{28}$	3.4
Nb–Ge[c]	23	$Cr_{73}Os_{27}$	4.7
Nb_3Sn	18	$Cr_{78}Rh_{22}$	0.07
Nb–Sb	2	$Cr_{82}Ir_{18}$	0.75
$Nb_{\sim 3}Bi$[b]	3	$Mo_{40}Tc_{60}$	13.4
$Ta_{\sim 3}Ge$[c]	8	$Mo_{\sim 65}Re_{\sim 35}$[c]	≃15
$Ta_{\sim 3}Sn$	8.3	$Mo_{75}Os_{25}$	13.1
$Ta_{\sim 3}Sb$	0.7	$Mo_{78}Ir_{22}$	8.5
Mo_3Al	0.58	$Mo_{82}Pt_{18}$	4.6
Mo_3Ga	0.76	$W_{\sim 60}Re_{\sim 40}$[c]	11
$Mo_{77}Si_{23}$	1.7		
$Mo_{77}Ge_{23}$	1.8		

a Rapid quenching b High-pressure synthesis c Film deposition techniques

The B1 crystal structure has a cubic unit cell with two kinds of atom. It is best thought of as a face-centered cubic array of anions with an interpenetrating fcc cation lattice (or vice-versa) so as to form a 3D checkerboard pattern as shown in Fig. 1.3. The cell looks the same whether you start with anions or cations on the corners. Each ion is 6-coordinate and has a local octahedral geometry. The most common of the B1 structure is that of NaCl.

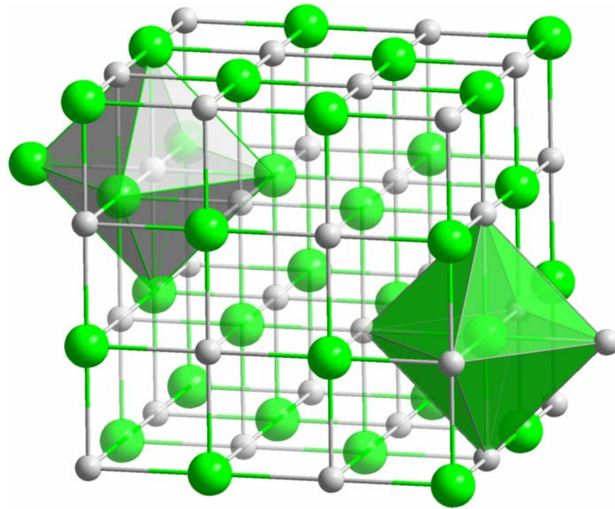

Fig. 1.3 The B1 crystal structure

The A15 crystal structure (also known as β-W or Cr_3Si structure types) is series of intermetallic compounds with the chemical formula A_3B (where A is a transition metal and B can be any element) and a specific structure. Many of these compounds have superconductivity at around 20 K, which is comparatively high, and remain superconductive in magnetic fields of tens of teslas. This kind of superconductivity (Type-II superconductivity) is an important area of study as it has several practical applications.

The first time of the A15 structure observed was in 1931 when an electrolytically deposited layer of tungsten was examined.[9] The discussion if the β–tungsten structure is an allotrope of tungsten or the structure of a tungsten suboxide was long-standing and in 1998 the articles about the discussion were still published. In the end it seems most likely that the material is a true allotrope of tungsten.[10]

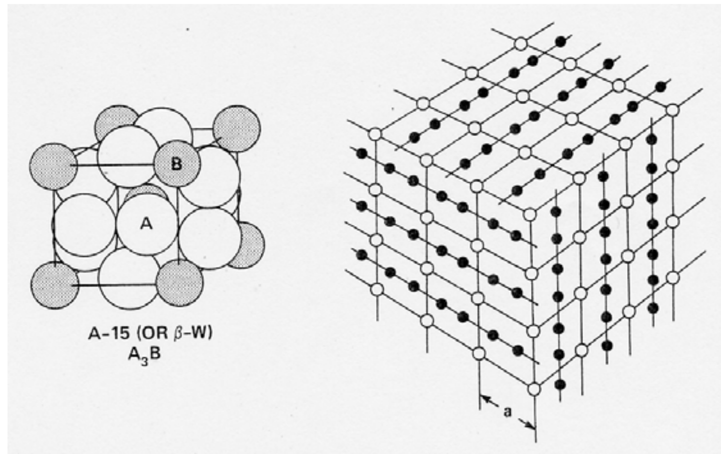

Fig. 1.4 The A15 crystal structure

The first inter-metallic compound with the typical A_3B composition was the chromium silicide Cr_3Si was discovered in 1933.[11] Several other compounds of the A15 structure were found in the following years. No large interest existed in the research on those compounds, but this changed with the discovery that Vanadium silicide V_3Si showed superconductivity at around 17 K in 1953.[12] In the following years several other A_3B superconductors were found.[13] Niobium-germanium held the record for the highest temperature of 23.2 K from 1971 till the discovery of the cuprates in 1986. Although some A15 phase materials can withstand higher magnetic field intensity and have higher critical temperatures than the NbZr and NbTi alloys NbTi is still used for most of the applications due to the easier manufacturing.[14] Nb_3Sn is used for some high field applications, for example high end MRI scanners and NMR spectrometers.

According to the Table 1.2 and Table 1.3, some candidates of high T_c material used for accelerator are: NbN, V_3Ga, V_3Al, Nb_3 Al, Nb_3Ge, V_3Si and Nb_3Sn. The compare of these materials [8] is shown as follow:

NbN:

Because of its high critical temperature of 17.2 K, NbN is the only B1 simple compound that has widely tested for accelerating cavities. Mainly two different techniques have been investigated: Thermal diffusion of N into Nb followed by rapid quench cooling and Reactive Sputtering onto Nb cavities. Rather seldom NbN applied to superconducting cavities gives better results than those obtainable by bulk Nb or Nb sputtered Cu. The main reason for this is the anomalously high resistivity of NbN in the normal state, which, even if not always reported in the

NbN cavities literature, is often higher than 100 μΩcm resulting into R_{BCS} and R_{RES} values larger than the expectancy.

NbN grains grow as columns perpendicular to the film plane, weakly bounded among each others, and separated by strong boundaries consisting of voids, normal conducting areas of Niobium and Niobium-dissolved gas composite phases like Niobium sub-Oxy-Carbo-Nitrides lumps. The denser is the grain boundary matrix, the higher is generally the normal state resistivity of NbN films. Resistivity values of the order of 1000 μΩcm are indeed encountered by sputtered films, with small average grain size, around 100 Å wide. Such films even show a strongly negative slope of resistivity against temperature that means RRR < 1 just as for semiconductors.

On the other hand T_C 's close to the maximum 17.3 K are monitored almost in correspondence of low resistivity values (100 μΩcm and RRR⩾1). The right B1-NbN superconducting phase is the so-called δ-phase corresponding to a lattice parameter of 4.388 Å and having a T_C very sensitive to Nitrogen stoichiometry. In sputtered films the δ-phase can be found mixed to some other low T_C phases like the α-Nb phase constituted by interstitial Nitrogen in bcc Nb lattice, the hexagonal (W_2C type) β-Nb_2N, the face centered tetragonal (distorted NaCl type) γ-Nb_4N_3 and the hexagonal (TiP type) ε-NbN phase.

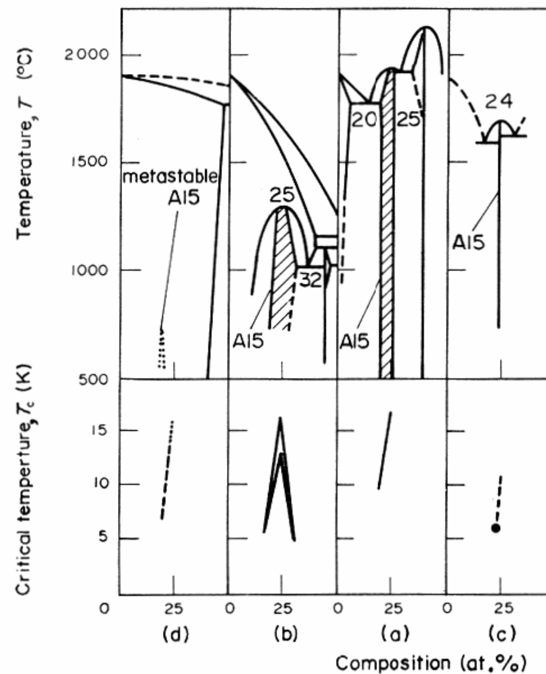

Fig.1.5 A15 phase fields and superconductivity in a) V-Si, b) V-Ga, c) V-Ge and d) V-Al Systems

Unfortunately even if no grain boundaries are present and a δ-phase single crystal is considered the single grain resistivity is not so low: A minimum value of ρ_n = 30μΩcm is expected, due to both metallic and gaseous vacancies in the lattice. This problem that is common to all the other B1 compounds consists in the fact that what corresponds to the equiatomic composition is not the formula $Nb_{1.0}N_{1.0}$, but $Nb_{0.987}N_{0.987}$: vacancies randomly distributed in both sublattices amounts to 1.3% respectively.

In order to improve the performance of NbN, the Titanium is added into. It presents all the advantages of the NbN, in the meanwhile it shows electrical conduction properties as more metallic as higher the titanium percentages is. Titanium is a good Nitrogen getter and the more Titanium we have the lower lattice vacancies will be. The Nitrogen stoichiometry hence is closer to 1 than for NbN. Moreover the critical temperature is even higher than that of NbN for Titanium content up to 40%. The resistivity instead decreases steeply versus the Titanium content [15-17]. This last phenomenon is the main reason under NbTiN choice. NbTiN cavities have been sputtered at CERN and at Saclay. The Q_0, at zero field, is higher than the Q-value of Niobium cavities, but the accelerating field achieved does not overcome the 10 Mv/m limit [18].

V_3Ga

The A15 phase forms by a congruent reaction from the bcc solid solution at 1295°C and is stable from 20 at. % to 32 at. % gallium. The T_C shows a marked maximum of 15.9K at stoichiometry and decreases almost linearly on both sizes. V_3Ga has the highest electronic density of states of all known A15 compounds. In contrast to the latter, however, it does not exhibit a low temperature phase transformation, which is explained by the fact that perfect ordering in this compound cannot be reached.

V_3Al

It shows a T_C up to 14K, but it is a metastable compound, superconducting only under thin film form. In principle metastability would be not a problem for RF applications construction, if V-Al is sputtered into a resonator, and moreover it has the advantage of a relatively low temperature of deposition. It should deserve further investigation, being a relatively little studied compound. The real problem indeed is that, because of metastability, this compound is not applicable to

superconducting magnet construction, and then it has been generally neglected in A15 treatises.

V_3Si

This material is one of the few examples of an A15 compound that form congruently from the melt. The A15 phase in the Vanadium-Silicon system is stable between 19 and 25 at. % Silicon. Large single crystals can be grown in the whole range either by zone melting or by recrystallization at 1870°C. There is a linear increase in T_C from 19 at. % to 25 at. % silicon, where a maximum T_C of 17.1K is achieved. For this compound, the RRR value of 80 can be obtained.

One problem must be solved before to apply this material to cavities: a proper substrate should be chosen. Niobium is not the right choice, because of the large diffusion coefficient of Vanadium into Niobium at high temperatures. The choice of Vanadium itself, as a substrate, should be more deeply considered, due to the drawback of lower thermal conductivity than Niobium, and this is a problem for the achievement of high gradients.

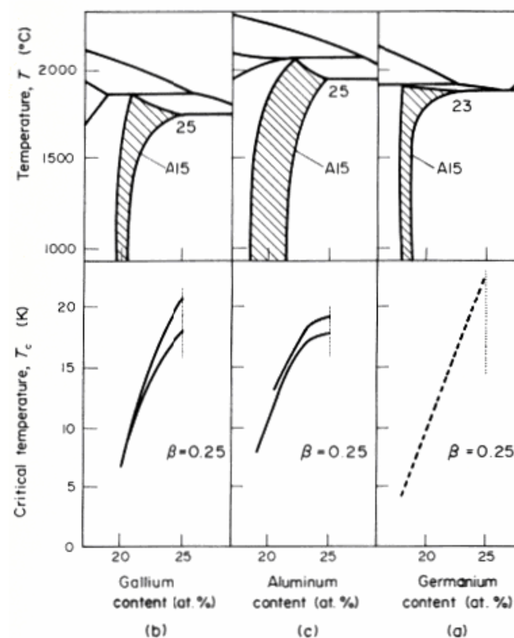

Fig.1.6 A15 phase fields and superconductivity in a) Nb-Ga, b) Nb-Ge, and c) Nb-Al Systems

Nb_3Al

This compound is formed by a peritectoid reaction from the bcc solid solution and sigma (Nb_2Al) phase at 1730°C, and contains 26 at. % Al. The

stoichiometric composition is metastable at room temperature and is only stable at 1940°C. The aluminium content of the A15 phase decreases with decreasing temperature; the homogeneity range at 1000°C is 19~22 at.% Al.

Nb_3Ge

The most striking feature of Nb_3Ge phase field is that the stoichiometric composition is not included at equilibrium, the highest solubility of Germanium being 23 at.%. At 1000°C, the homogeneity range of the A15 phase is very narrow and is centered at 18 at.% with total width of 1 at.%. It has not been possible to rise T_C above 17~18 K in bulk sample either by quenching or other means. Metastable stoichiometric, or near stoichiometric, Nb_3Ge can be prepared as thin films with critical temperature of 23 K. But the big problem is that the material is very brittle, which meaning is that a strike or vibration can change the A15 structure and cease the superconductor.

Nb_3Sn

Nb_3Sn is the only A15 material that has given promising results when applied to the construction of a real cavity [19]: Tin was reactively diffused into an Nb bulk cavity and the Q-factor was in the order of 10^{11}, the accelerating field being limited to about 12 MV/m.

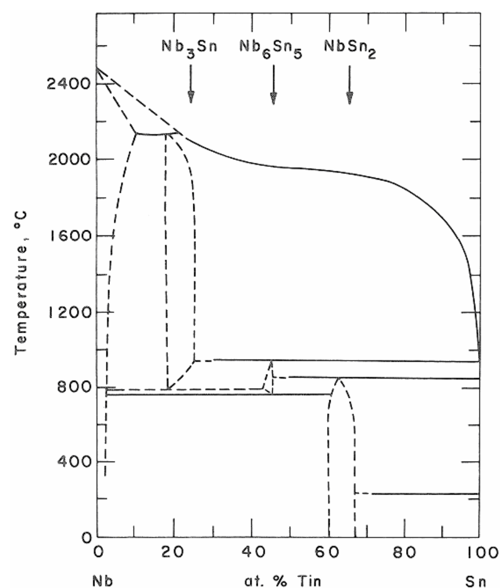

Fig.1.7 The Niobium-Tin phase diagram

According the phase diagram of Fig. 1.7, the A15 phase is unstable below

775°C. From the same diagram, it is seen that several spurious phases are also possible, and this can represent a limitation for the fabrication of superconducting cavities. Besides T_C, however for Nb-Sn system there is another quantity undergoing a much stronger variation in the narrow composition range between 24.5 at. % and 25 at.% Sn: the resistivity in normal state just before transition. Resistivity indeed changes from 20 μΩ cm at 24.4 at. % tin to less than 4 μΩcm at 25 at.% tin; this sharp change being a direct consequence of the perfectly ordered state of Nb_3Sn. This consideration is absolutely critical: for everybody wishing to carry on further investigation on Nb_3Sn, it is mandatory to look for low resistivity. The parameters comparison between Nb and Nb_3Sn are shown in Table 1.4[1].

Table 1.4 the parameters of Nb_3Sn and Nb

Property	Nb	Nb_3Sn
T_c [K]	9.2	18
$\mu_0 H_{c1}(0)$ [T]	0.17	0.038
$\mu_0 H_c(0)$ [T]	0.2	0.52
$\mu_0 H_{c2}(0)$ [T]	0.4	30
$\xi_{GL}(0)$ [nm][b]	29	3.3
$\lambda_{eff}(0)$ [nm][c]	41	135
$\kappa(0)$[d]	1.4	41
$\Delta(0)$ [meV][e]	1.4	3.4
ρ_n [$\mu\Omega$cm]	< 100	< 20

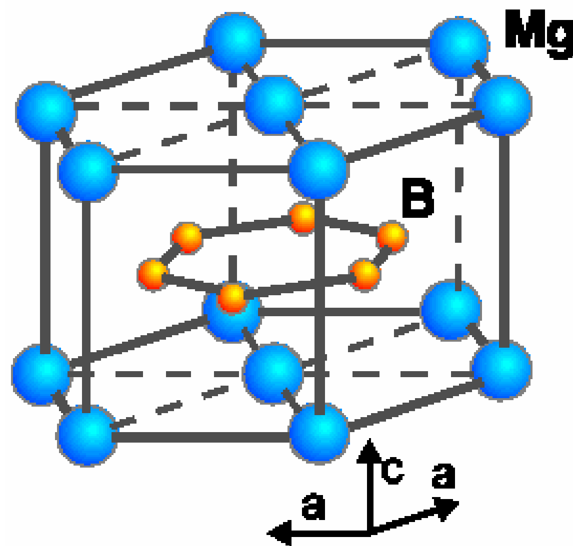

Fig 1.8 the crystal structure of MgB_2

Another important new superconductivity material is the magnesium diboride

(MgB_2), which is a simple ionic binary compound that has proven to be an inexpensive and useful superconducting material. Its crystal structure is shown in Fig. 1.8.

The superconductivity of MgB_2 was announced in the journal Nature in March 2001 by Nagamatzu and Akimitsu [20]. Its Tc of 39 K for a sp-bonded is the highest amongst conventional superconductors. This material was first synthesized and its structure confirmed in 1953,[21] but its superconducting properties were not discovered until 2001. The discovery caused great excitement and led to the general interest in this material, since it opens the way to a new class of simple and low-cost binary intermetallic superconductors with a record HTCs for non-oxide and non C-60 based compounds.

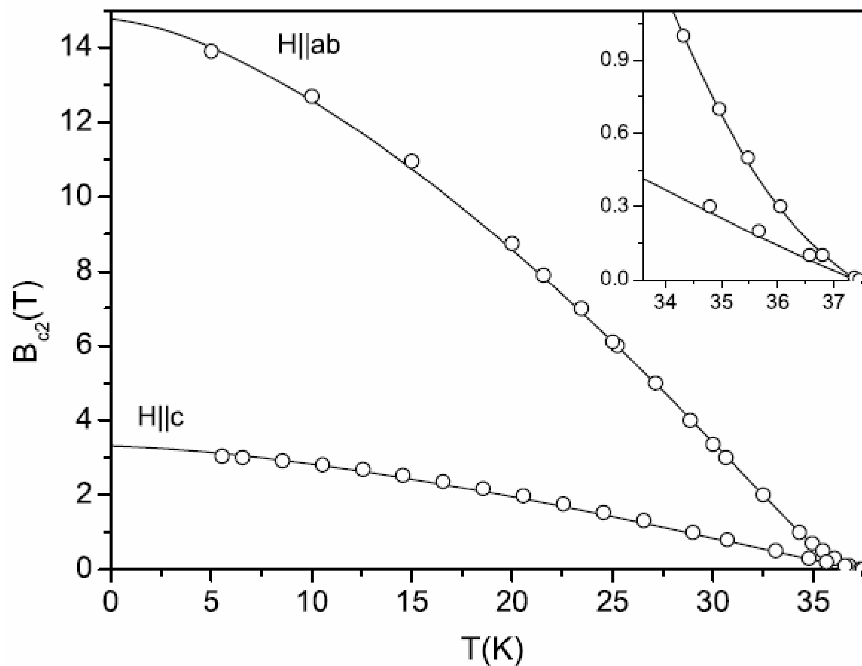

Fig. 1.9 Temperature dependence of the upper critical field, the region near T_c is enlarged in the inset.

Though generally believed to be a conventional superconductor and most experimental works, as Raman Spectroscopy, Boron-isotope effect, Spin lattice relaxation time, tunneling measurements and optical conductivity data, are all consistent with the existence of phonon mediated superconductivity, it is a rather unusual one. But an unusual superconducting gap behavior has been observed indicating the existence of a double gap [22] and the presence of a smaller gap is a serious drawback for RF applications. Its electronic structure is such that there exist

two types of electrons at the Fermi level with widely differing behaviours, one of them (σ-bonding) being much more strongly superconducting than the other (π-bonding). This is at odds with usual theories of phonon-mediated superconductivity which assume that all electrons behave in the same manner. Theoretical understanding of the properties of MgB_2 has almost been achieved with two energy gaps. It was regarded as behaving more like a metallic than a cuprate superconductor.

On the other side the material appears promising for RF, since it is rather insensitive to impurity content; it is highly metallic and has strong linked grain boundaries. Its properties depend greatly on composition and fabrication process. Many properties are anisotropic due to the layered structure. 'Dirty' samples, e.g., with oxides at the crystal boundaries, are different from 'clean' samples.[23]

The maximum critical current (Jc) is: 10^5 A/m² at 20 T, 10^6 A/m² at 18 T, 10^7 A/m² at 15 T, 10^8 A/m² at 10 T, 10^9 A/m² at 5 T[23].

Up to 2008, the parallel upper critical field (H_{c2}) obtained is about 14.8 T, and the perpendicular upper critical field is about 3.3 T as shown in Fig. 1.10[23]. In thin films the field is up to 74 T, and in fibres up to 55 T[23].

MgB_2 thin film produced by the hybrid physical chemical vapour deposition (HPCVD) has the good performance, which characterized by T_{c0} = 41.8 K, ρ_0 = 0.26 μΩ cm, RRR > 30 [24,25], and self-field $J_c = 3.4\times10^7$ A cm^{-2} [26].As far as superconducting cavities are concerned, still many problems must be solved: the degradation of superconducting properties of MgB_2 after the immersion in water.

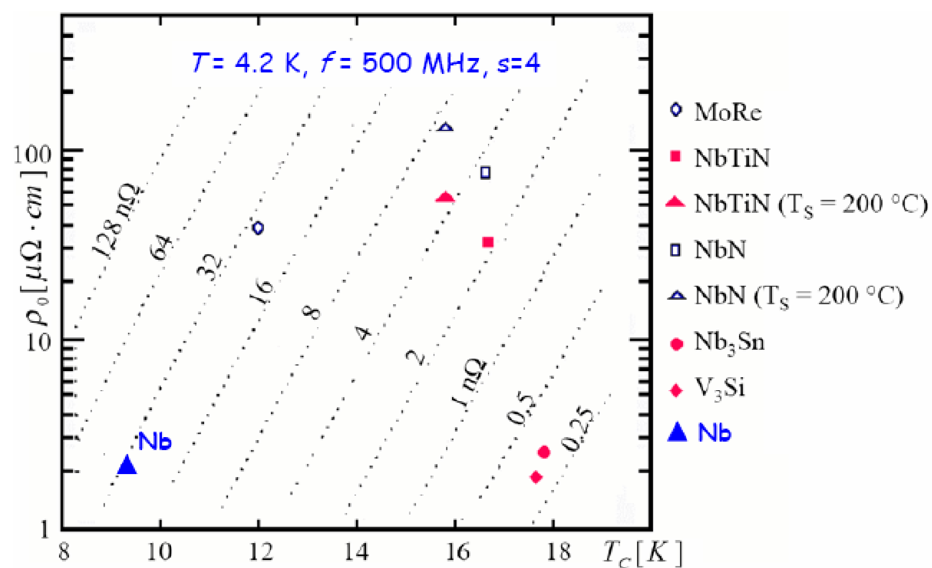

Fig.1.10 R_{BCS} of different material

In order to compare the R_{BCS} of different material, the nomogram [8,27] of Fig. 1.10 can be constructed for materials at 4.2 K, 500 MHz and a strong coupling factor of 4. Chosen a certain value of R_{BCS}, on the corresponding curve there are all the materials with different T_C and ρ_n having the same R_{BCS}. Among the material described in Fig. 1.10, the ρ_0 of V_3Si and Nb_3Sn is the most small. Although the T_c of MgB_2 is higher than that of V_3Si and Nb_3Sn, its R_{BCS} is the same order of that of V_3Si and Nb_3Sn because of the 2.3 meV energy gap of π bonding at 4.2K [28]. So, among these three kinds of material, Nb_3Sn is the most stable and easy to obtain.

The last problem is that why we used the thin film for the superconductor cavity. The first reason is that it is possible to use different substrates, which can improve the thermal stability and the mechanical stability. For example, the thermal conductivity and mechanical performance can be improved by the Cu substrate. The second reason is to reduce the manufacture cost and the consuming of the superconductivity material. The third reason is to improve the performance of the superconductor, such as the T_c, RRR, Q value, H_c and so on. For example, the performance of the MgB_2 thin film is better than that of the bulk of Nb most. But this is not always effective. For example, the Q value of the thin film Nb cavity is higher than that of bulk Nb cavity at low accelerator field, but it is always reversed at high field [29].

In other words, the thin film cavity always has a higher Q-slope, especially for innovative superconductors. However, some kinds of superconductivity material can not be used to shape the cavity by the bulk material because the material is brittle and the distortion can change the crystal lattice to change the superconductivity performance, such as Nb_3Sn, MgB_2, and so on.

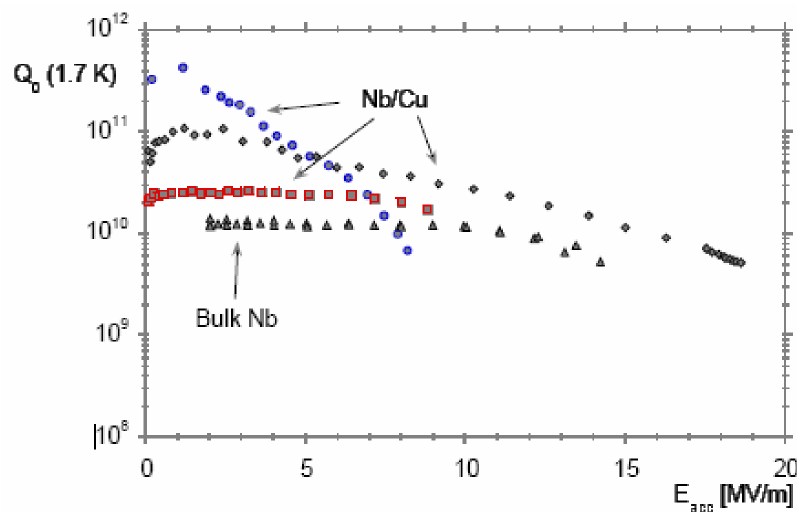

Fig.1.11 the Q_0 of Nb

Of course, there are some other kinds of superconductor, such as organic superconductor, molecular superconductor and high temperature superconductor. The RRR of organic superconductor is lower, so it is not proper to be used for the accelerator cavity because of higher R_{BCS}. The thin film of the molecular superconductor is some difficult to be obtained. The critical H and the critical current of the high temperature superconductor are somewhat lower than that of accelerator cavity needed.

In the conclusion, the Nb_3Sn thin film is very important for the superconductor cavity. There are two methods to manufacture the Nb_3Sn thin film: the diffusion method and multilayer deposition method. In this thesis, we focus on the multilayer deposition method.

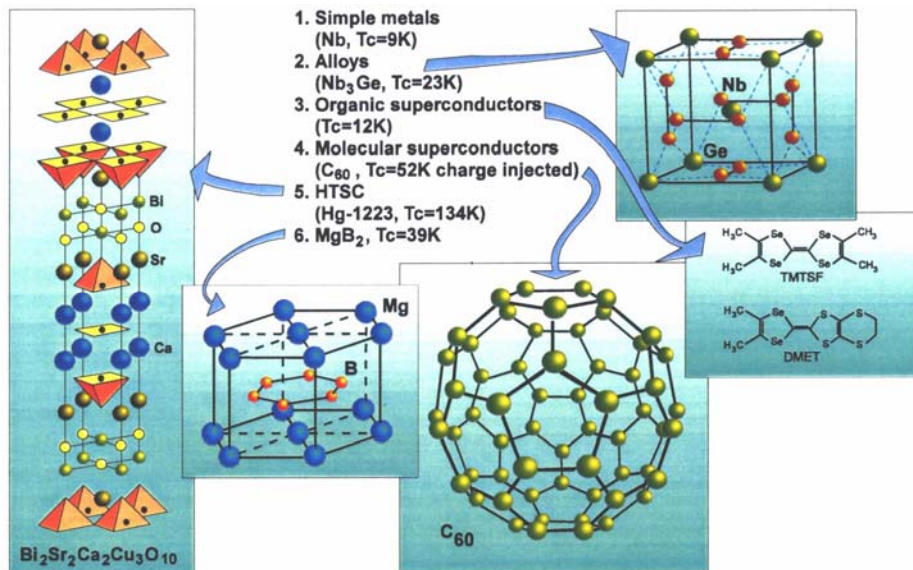

Fig.1.12 the different kinds of supercondoctor

Chapter 2 Introduction: How to sputter Nb thin film

2.1 Technique of the vacuum

From the Eq.(1.6), the RRR of the same material is determined by the residual surface resistance, which is fundamentally determined by the purity of the thin film. The method to improve the purity is to improve the base pressure of the sputtering chamber. So the ultra high vacuum (UHV) system is needed for obtaining the vacuum pressure higher than 10^{-7} mbar. The vacuum system is shown as Fig. 2.1 and Fig. 2.2.

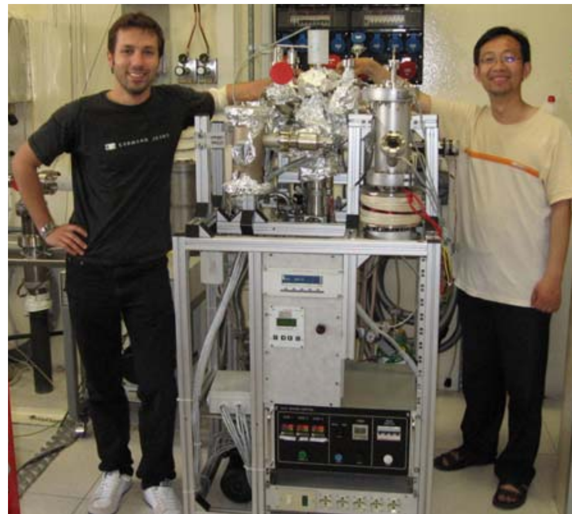

Fig. 2.1 the front view of the system

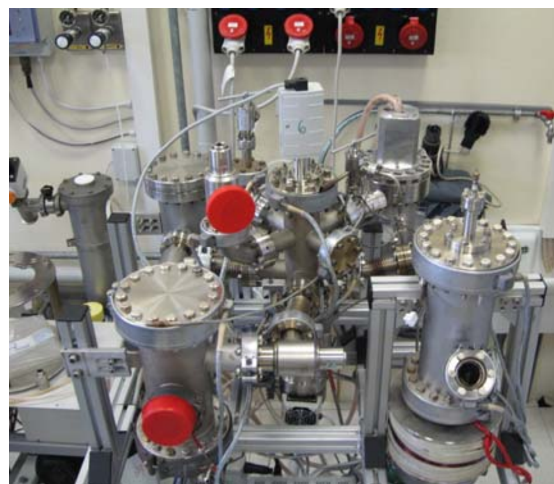

Fig. 2.2 the top view of the system

The UHV system is composed of four operation chamber and one main chamber

as shown in Fig.2.3. The four operation chamber is linked with the main chamber by all metal valves. The main chamber is pumped by the turbomolecular pump and rotary pump. The gate valve is used for separating the main chamber and the pump. The nitrogen linked by the venting valve is used for venting the vacuum. The argon linked by the leak valve is the sputtering proceeding gas. A vacuum gauge is used for measurement the pressure of the main chamber. The chamber 1 is used for the sample deposition by magnetron. The chamber 2 is used for 6 GHz cavity deposition. The chamber 3 is used for annealing by an inductor. The chamber 4 is used for annealing by a lamp. The 3 dimensional design of the system by the Inventor is shown as Fig.2.4.

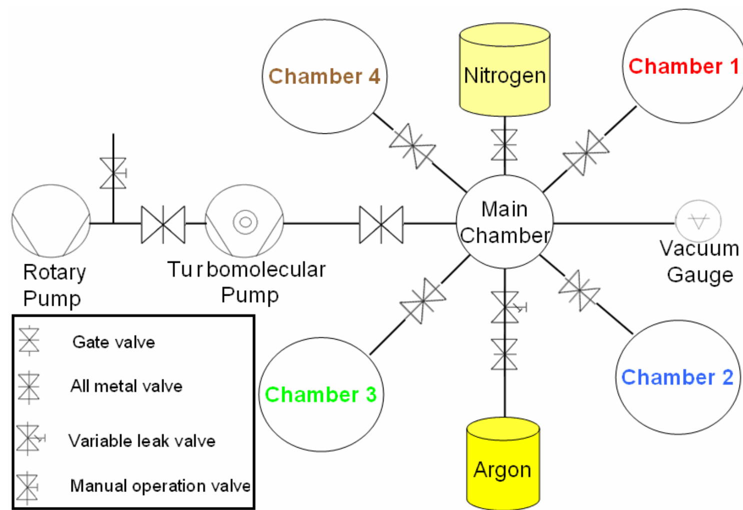

Fig. 2.3 the scheme of the UHV system

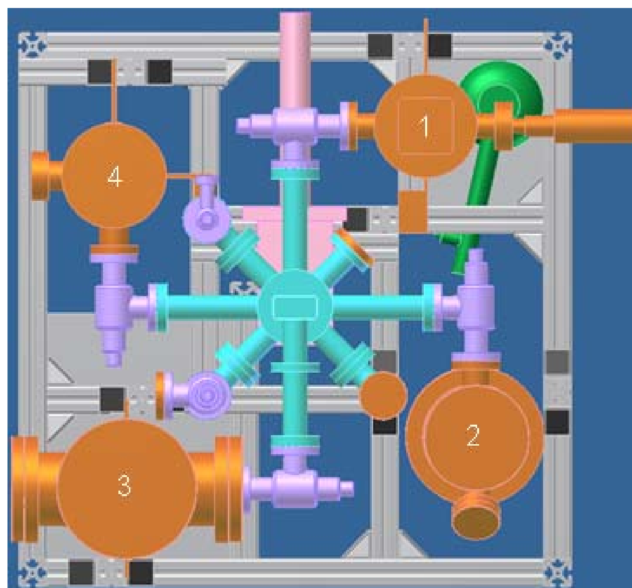

Fig. 2.4 3-Ddesign of the UHV system

The UHV system is controlled by the control panel, which include the controller of the pump, the switch of the gate valve, the controller of the baking system, the controller of the inductor annealing system and the vacuum display.

Fig. 2.5 Control panel

Fig.2.6 Vacuum gauge

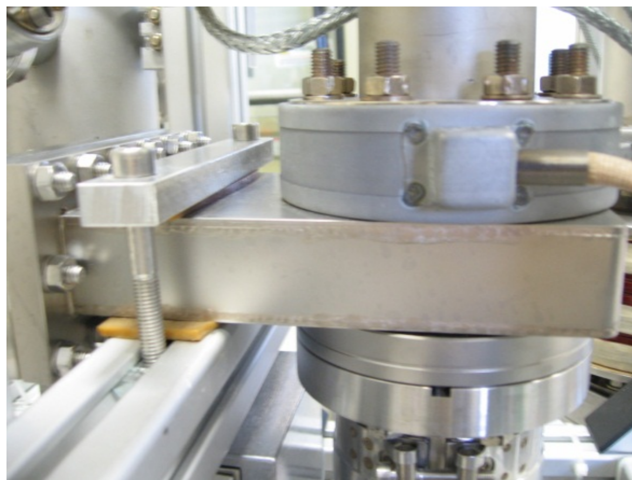

Fig.2.7 Gate valve

Fig.2.8 turbomolecular pump

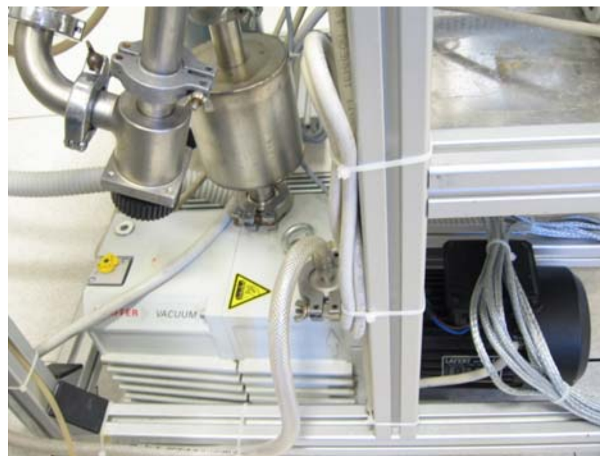

Fig. 2.9 Rotary Pump

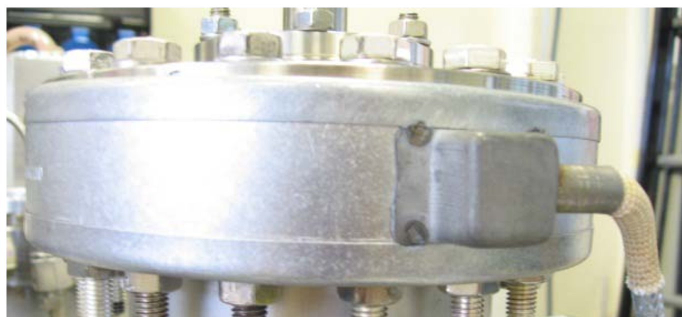
Fig.2.10 Heating Element

Before pumping the system, we first open the all metal valve of the used chamber, and close that of other chamber. We also need to close the all metal leak valve of Ar and N_2. And then, we open the gate valve, press starting pump button, and switch on the gauge.

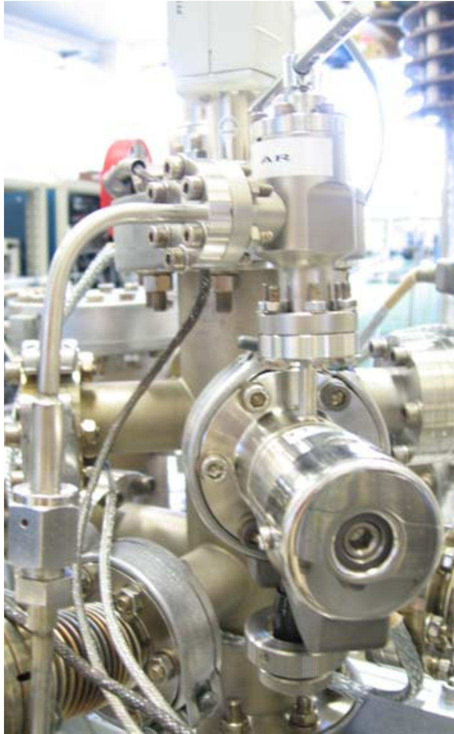

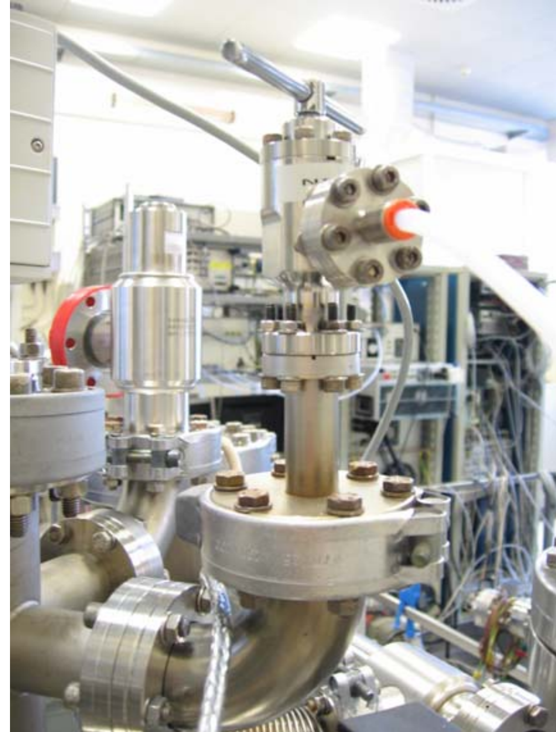

Fig.2.11 Argon leak valve and all metal valve   Fig.2.12 Nitrogen Vent Valve

Fig. 2.13 Argon Bottle

Fig. 2.14 The chamber covered with aluminum foils.

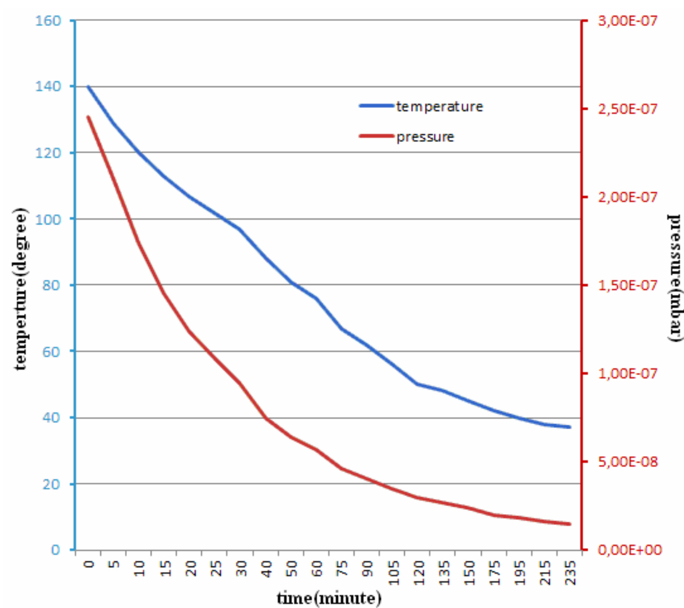

Fig. 2.15 The cooling curve after baking.

In order to reduce the pumping time, the system baking is needed for obtaining the UHV higher than 10^{-7} mbar. We must wait the pressure up to 10^{-6} mbar before start baking in order to be sure that the system don't have big leak. In order to obtain the

uniform baking temperature and better baking, we cover the main chamber and the chamber that you want to use with aluminum foils. The vacuum gauge can not be covered. And then, we set the temperature of baking and the time of baking.

It should be sure that thermocouples are connected to their own zones and heat only the chambers that you are pumping, and we should not set T>120℃ if you have mounted windows, magnetrons and viton o-rings. The cooling water should be given before the baking start for the protection of the permanent magnet. When the baking is finished, we wait for the natural cooling of the system till it near the room temperature. From the cooling curve of Fig.2.15, the pressure decrease with the temperature decreasing.

2.2 Nb thin film on sapphire

In order to research the performance of the thin film and the parameters of sputtering, the Nb thin film on sapphire should be first researched.

2.2.1 Sputtering configuration

Fig.2.16 The assembly of the Nb magnetron

The sputtering is proceeded by a 2 inch of magnetron, which of component is shown as Fig.2.16. The magnetron is mounted with a new copper gasket from the bottom of the sputtering chamber after cleaning with acetone and alcohol. A flange with glass window is mounted from the top of the chamber.

Fig. 2.17 the gasket and the magnetron

Fig. 2.18 mounting the magnetron from the bottom of the chamber

Fig. 2.19 the flange with glass window

Fig. 2.20 the ultrasonic cleaning machine

Fig. 2.21 preparation of the sapphire fixing on the holder

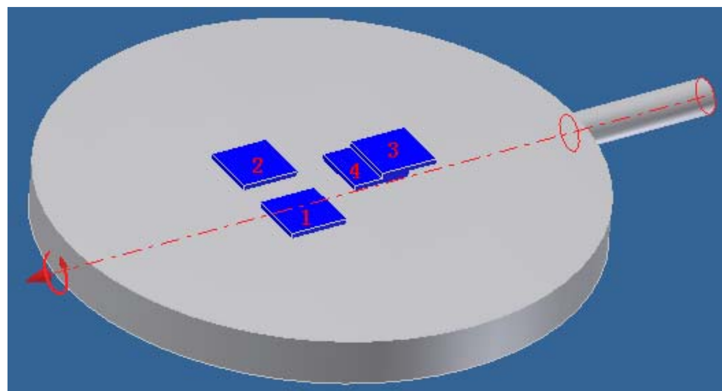

Fig. 2.22 the sample and its holder

The sapphire sample is needed to clean with ultrasonic for better adhering with the thin film. The sample is fixed on the aluminum sample holder with silver paint as

shown in Fig. 2.21 and Fig. 2.22. The distance between the sample and the magnetron is about 7 cm.

2.2.2 Deposition parameter

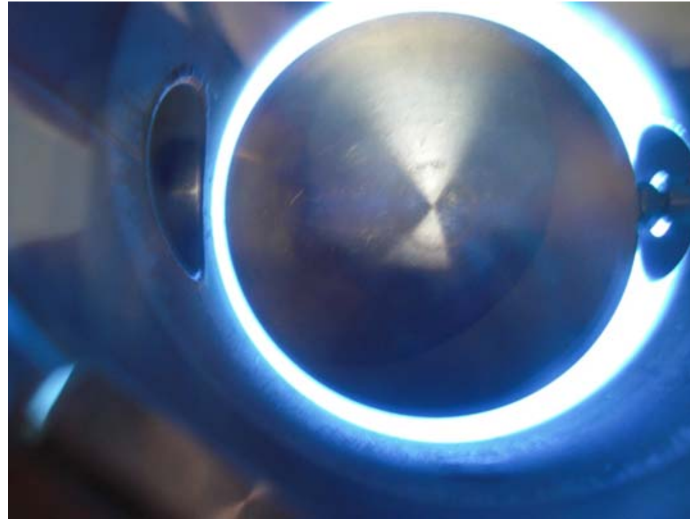

Fig. 2.23 The plasma during the sputtering

We should use the different sputtering parameter to research the performance of the thin film. The main sputtering parameters include the sputtering current, the deposition time and the proceeding pressure. In our experiment, the three parameters are all changed as shown in table 2.1.

Table 2.1 The sputtering parameters

run	Time(min)	Current(A)	Gas pressure (mbar)
1	25	0.8	$5*10^{-3}$
2	20	1.0	$5*10^{-3}$
3	15	1.2	$5*10^{-3}$
4	15	1.4	$5*10^{-3}$
5	20	1.0	$3*10^{-3}$
6	20	1.2	$3*10^{-3}$
7	20	1.4	$3*10^{-3}$

2.2.3 Analysis and results

2.2.3.1 Thickness measurement

We use the sample 4 of each run to measurement the thickness of thin film. Each of the sample is deposited the thin film on about half of the surface area. We measurement the thickness of each sample five times and average the result.

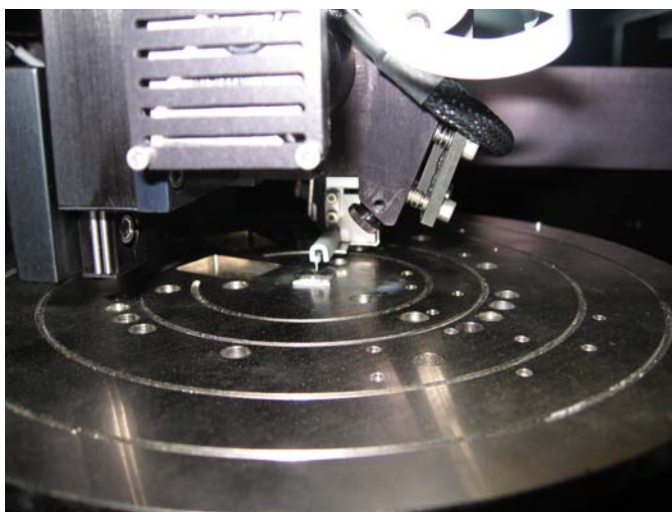

Fig. 2.24 the profile measurement machine

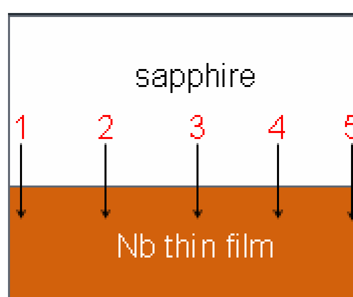

Fig. 2.25 The measurement trace

Table 2.2 The thickness measurement results

run	Time(min)	Current(A)	Gas pressure (mbar)	Thickness(nm)	Deposition rate (nm/s)
1	25	0.8	$5*10^{-3}$	1660	1.4
2	20	1.0	$5*10^{-3}$	2100	1.7
3	15	1.2	$5*10^{-3}$	1750	1.9
4	15	1.4	$5*10^{-3}$	2080	2.3
5	20	1.0	$3*10^{-3}$	1920	1.6
6	20	1.2	$3*10^{-3}$	2480	2.1
7	20	1.4	$3*10^{-3}$	2610	2.2

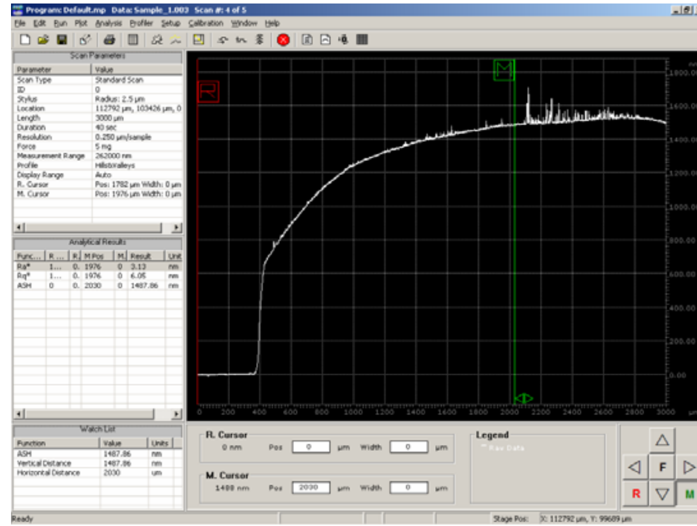

Fig. 2.26 The interface of the surface profile measurement

According to the results, the deposition rate is proportion to the sputtering current and the proceeding gas pressure, which means that the deposition time determines the thickness of the thin film and the sputtering current determines the deposition rate,

2.2.3.2 Tc measurement

In order to measurement the critical temperature (T_c), we should use the liquid Helium, because only the liquation point of He (4.2K) is lower than the T_c of Nb.

We use the four point resistance measurement method to measure the T_c[30]. The four contacting point are arranged as the last one in Fig. 2.29 by a spring as shown in Fig.2.30. The input current is fixed at 10 uA and changed its direction in period of 1 second. In the T_c measurement instrument, the sample is place on a piece of paper painted with grease for the good thermal conductor, and the sample should be prevented to contact with copper directly.

Because the measurement error and the phase change process, the temperature of changing from the normal conductor to superconductor is not a point value. In order to minimizing the error, we calculate the T_c and dT_c as follow:

$$T_C = \frac{T_{C90\%} + T_{C10\%}}{2} \tag{2.1}$$

$$dT_C = \frac{T_{C90\%} - T_{C10\%}}{2} \tag{2.2}$$

Fig. 2.27 450*l* liquid He Dewar

Fig. 2.28 the current source and voltage meter for T_c measurement

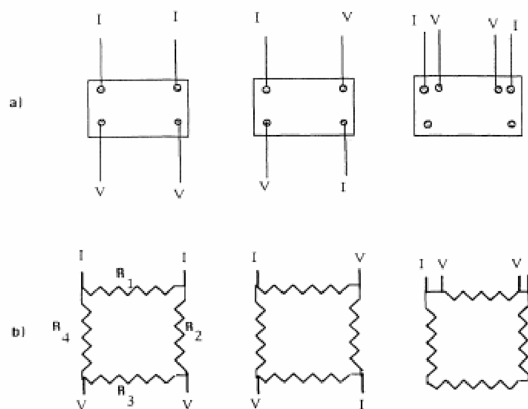

Fig. 2.29 the different arrangement of four point resistance measurement

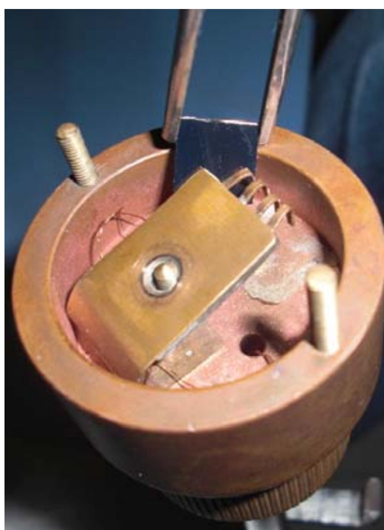

Fig. 2.30 put the sample into the T_c measurement set up

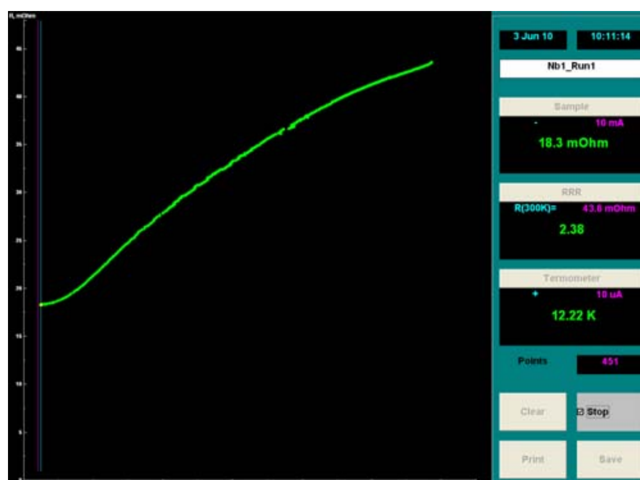

Fig. 2.31 the interface of Tc measurement high than 10K

Fig. 2.32 the interface of Tc measurement less than 10K

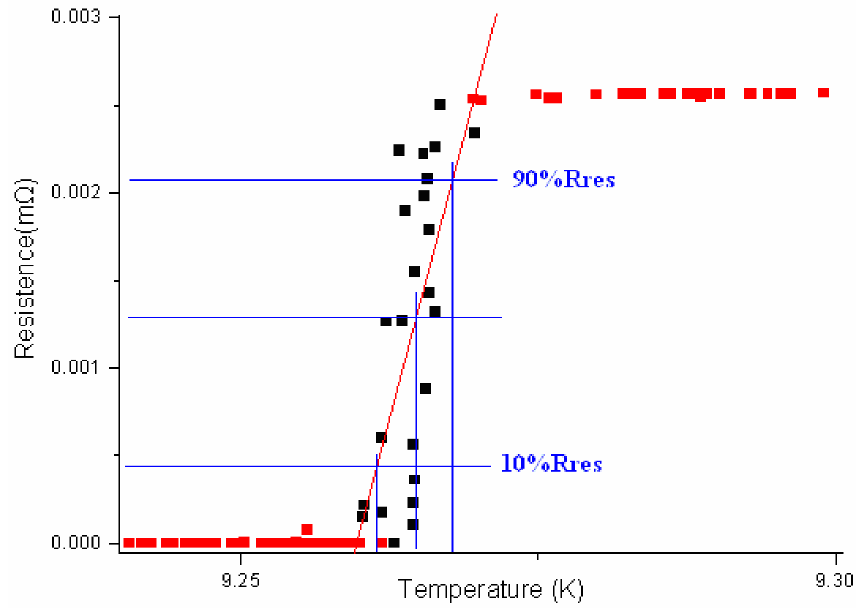

Fig. 2.33 the fitting of the Tc curve

Table 2.3 the results of T_c measurement

sample	Tc(K)	dTc(K)	RRR	Pressure (mbar)
r1s1	9.18	0.0017	9.10	5*10^-3
r1s2	9.17	0.0015	8.61	5*10^-3
r1s3	9.19	0.0136	9.01	5*10^-3
r2s1	9.27	0.0049	7.88	5*10^-3
r2s2	9.20	0.0092	7.69	5*10^-3
r2s3	9.25	0.0121	7.99	5*10^-3
r3s1	9.26	0.0054	7.65	5*10^-3
r3s2	9.26	0.0160	9.39	5*10^-3
r3s3	9.27	0.0053	6.00	5*10^-3
r4s1	9.26	0.0040	10.94	5*10^-3
r4s2	9.23	0.0064	9.60	5*10^-3
r4s3	9.26	0.0092	9.91	5*10^-3
r5s1	9.02	0.0219	18.60	3*10^-3
r6s1	9.05	0.0032	10.40	3*10^-3
r6s2	9.02	0.0159	19.20	3*10^-3
r6s3	9.04	0.0107	17.60	3*10^-3
r7s1	9.05	0.0068	15.90	3*10^-3
r7s2	9.05	0.0138	13.00	3*10^-3
r7s3	9.06	0.0056	12.50	3*10^-3

Where, $T_{c90\%}$ is the temperature of 90% of the residual resistance, $T_{c10\%}$ is the temperature of 10% of the residual resistance, and dT_c is the range of T_c. The measurements of the T_c are shown as in Table 2.3. Where, r1s2 means the second sample of the first run. According to the results, the proceeding gas pressure affects the performance of the thin film, RRR.

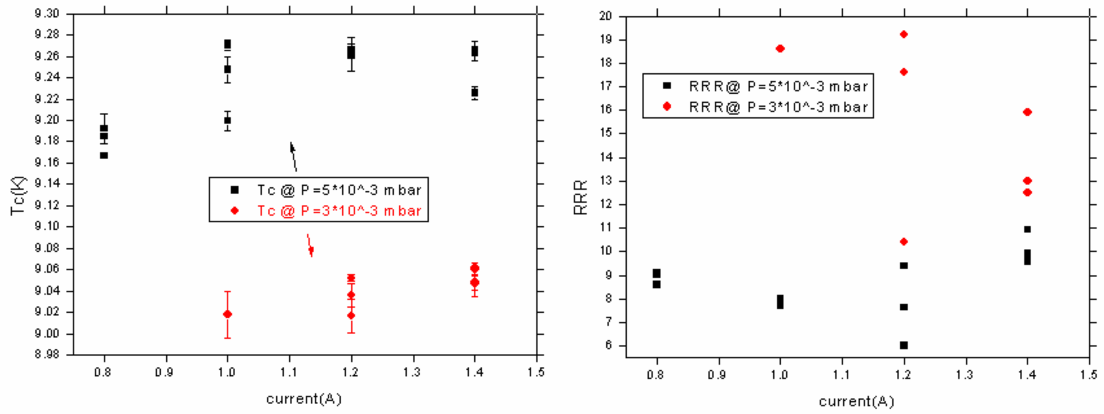

Fig. 2.34 the performance of the thin film

In the Fig. 2.34, the T_c of the sample deposited at the pressure of $5*10^{-3}$ mbar are higher that at the pressure of $3*10^{-3}$ mbar, but the RRR of the sample deposited at the pressure of $5*10^{-3}$ mbar are lower than that at the pressure of $3*10^{-3}$ mbar. This means that the lower pressure can improve the purity of the thin film and decrease the T_c. However, the reason is needed to research.

2.2.3.3 XRD analysis

In order to research the crystal structure of the thin film, we should do the X ray diffraction (XRD). From the result of the XRD, we can obtain the crystal plane, and then we can get the information of the thin film.

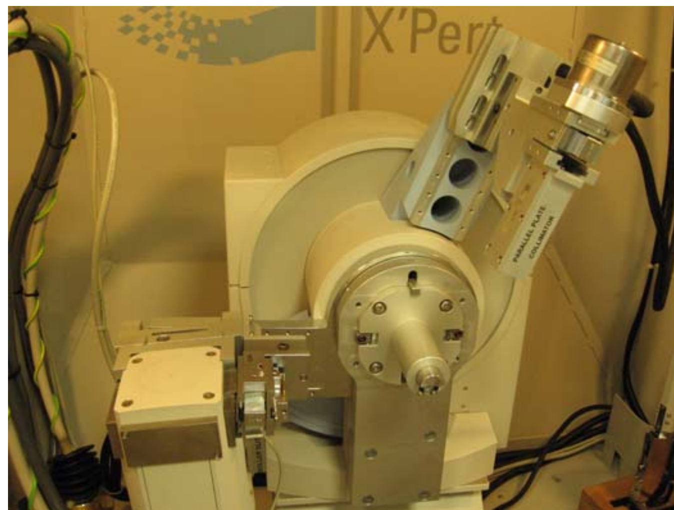

Fig. 2.35 The XRD machine

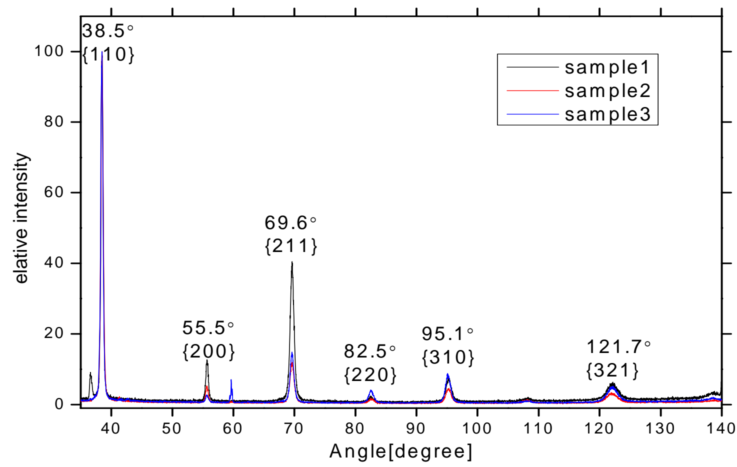

Fig. 2.36 the XRD result of Run 1

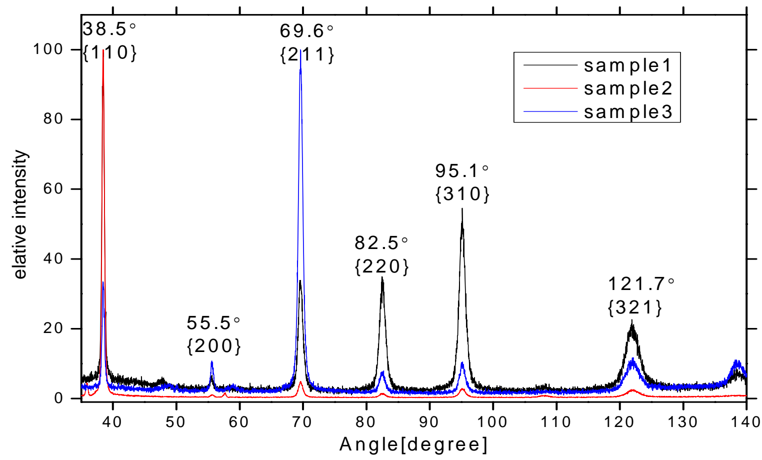

Fig. 2.37 the XRD result of Run 2

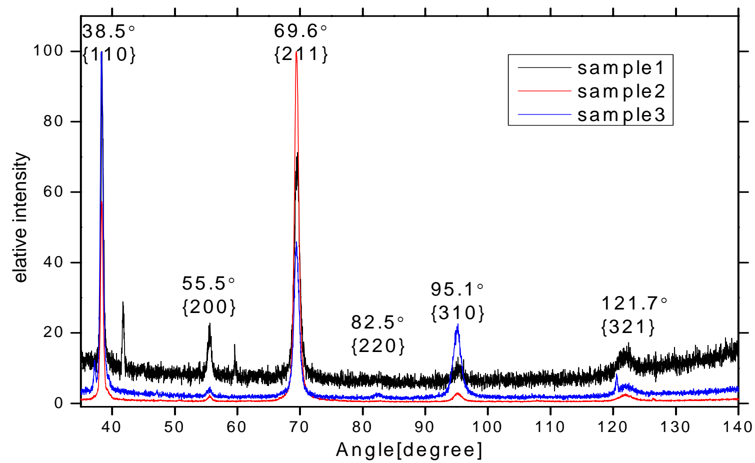

Fig. 2.38 the XRD result of Run 3

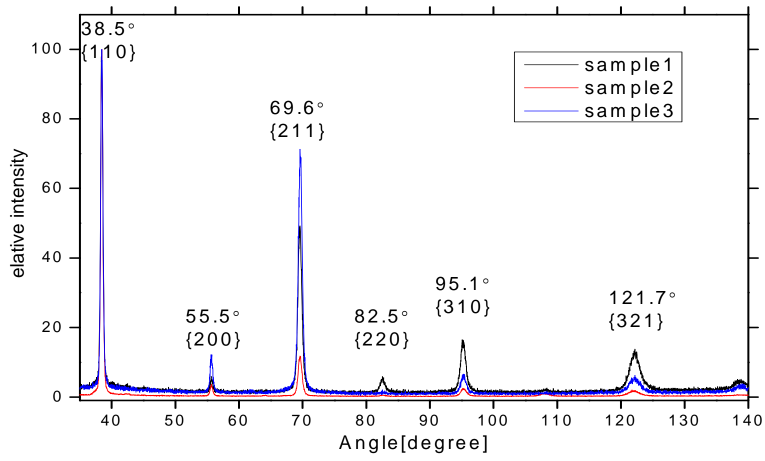

Fig. 2.39 the XRD result of Run 4

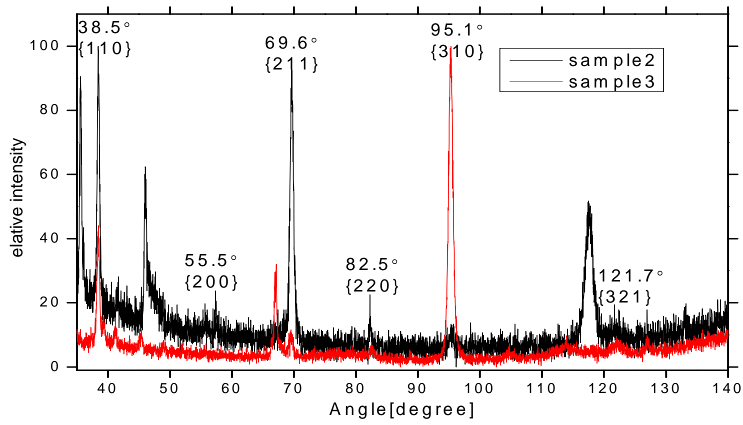

Fig. 2.40 the XRD result of Run 5

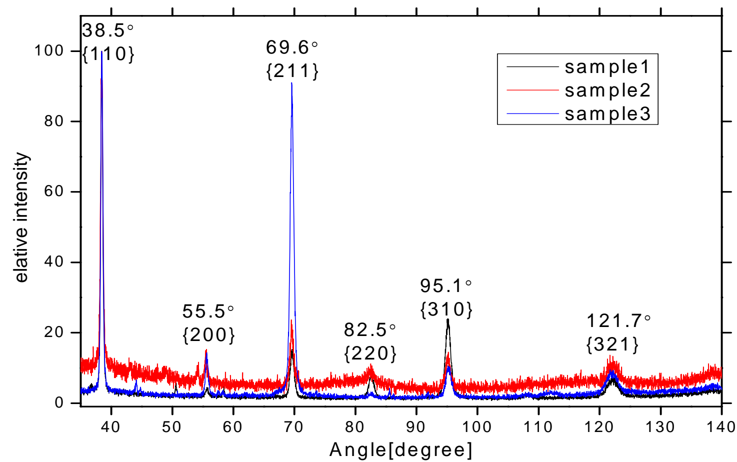

Fig. 2.41 the XRD result of Run 6

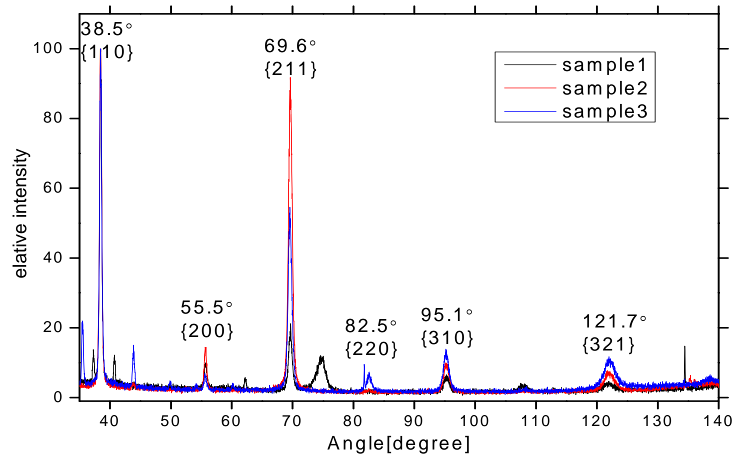

Fig. 2.42 the XRD result of Run 7

According to the result of the XRD experiment from Fig. 2.36 to Fig. 2.42, there are some abnormal peaks, such as {211} of sample2 of run3, {211} of sample3 of run2. All of the marked peaks are the crystal plane of the Nb. The unmarked peaks of Run 3 sample 1 may be that of Oxygen element, the unmarked peaks of Run 7 sample 1 may be that of NbO, and the unmarked peaks of Run 5 sample 2 may be that of NbO and Oxygen, which should be investigated in the next step.

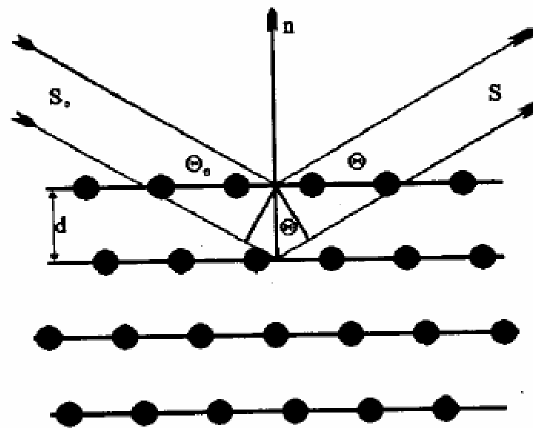

Fig.2.43 The mirror reflection of the photon

The peaks of the figures of the XRD results are formed by the crystal, which can be explained by W. H. Bragg as shown in the Fig.2.43. If we regard the crystal planes as mirrors, constructive interference is observed when the path difference between the two reflected beams is $n\lambda$. The path difference of the photon action on the adjacent crystal plane is:

$$2d\sin\theta = n\lambda \tag{2.3}$$

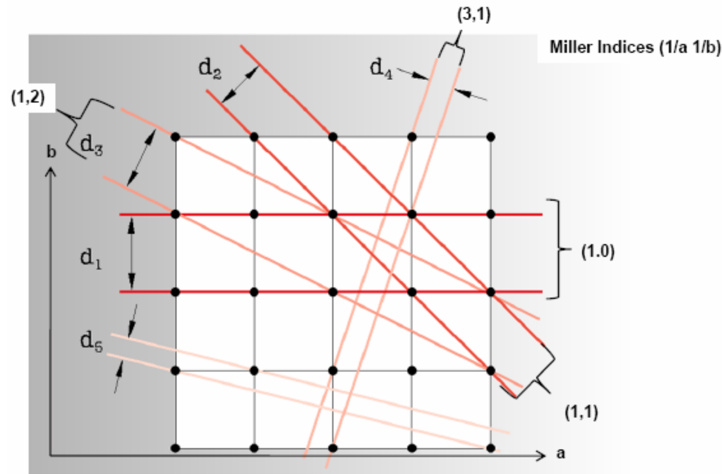

Fig.2.44 the different distance of the different crystal plane

Where d is the interplanar spacing. However, the distance is different with the different crystal plane as shown in Fig.2.44. For the cubic crystal, there is a relationship:

$$\frac{1}{d_{(h,k,l)}{}^2} = \frac{(h^2+k^2+l^2)}{a^2} \tag{2.4}$$

Where, h,k,l stand for the direction of the crystal plane, a is the cubic edge length. And then we have:

$$\frac{4\sin^2(\theta)}{n^2\lambda^2} = \frac{(h^2+k^2+l^2)}{a^2} \tag{2.5}$$

According to the Eq.(2.4), Eq.(2.5) and the XRD results from Fig.2.35 to Fig.2.42, we can obtain the d-space of {110} crystal plane, and then the cubic edge length can be obtained of each sample as shown in Table2.3.

Table2.3 the cubic edge length of each sample

Run	1	2	3	4	5	6	7
Sample 1 [Å]	3.308439	3.31107	3.315595	3.311636		3.317066	3.310434
Sample 2 [Å]	3.308793	3.310504	3.319626	3.311749	3.3109	3.31264	3.311126
Sample 3 [Å]	3.319089	3.309868	3.322016	3.311593	3.313106	3.311211	3.310391
Average [Å]	3.312107	3.310481	3.319079	3.311659	3.312003	3.313639	3.31065

The relationship between the cubic edge length and sputtering current is shown in Fig.2.45, where the black point means that the pressure of proceeding gas is

5*10^{-3}mbar and the red point means 3*10^{-3}mbar. From the picture, we can see that the highest cubic edge length is that of 1.2 A sputtering current.

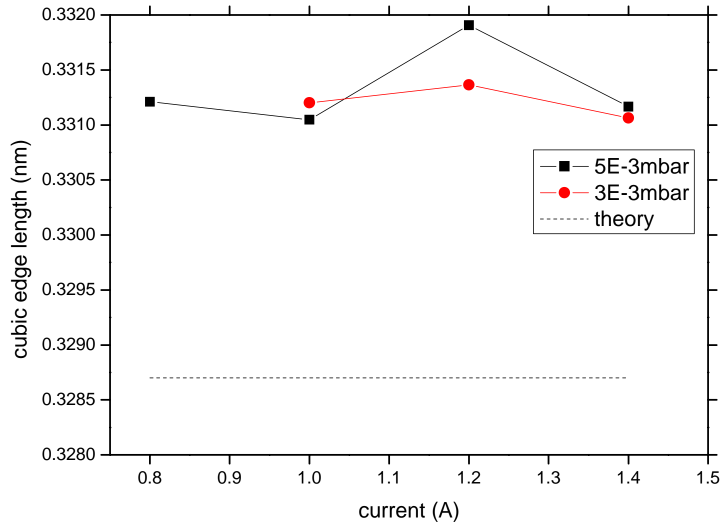

Fig. 2.45 the cubic edge length versus sputtering current

2.3 Discussion

Sample analysis of sputtered niobium films is the primary step for the Nb_3Sn multilayer thin film deposition. Film crystalline structure, thickness, T_c and RRR are important diagnosis of the sputter deposition. The further investigation is needed.

Chapter 3 Multilayer deposition of Nb_3Sn

3.1 Technique of deposition

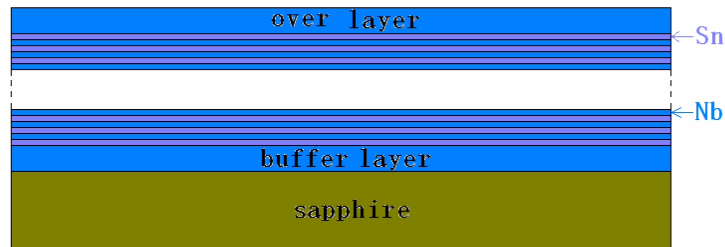

Fig. 3.1 the structure of multilayer

Multilayer deposition can improve the H_c of superconductor. However, we use the multilayer to produce the A15 crystal structure of Nb_3Sn. If the thin film is made of multilayer as shown in Fig. 3.1, when we heat the thin film, the Sn atom and the Nb atom move little distance and the A15 Nb_3Sn crystal is easy to be obtained. In order to improve the adherence of the thin film, the Nb buffer layer is first deposited. Because the vapour pressure of Sn is very low, the Nb over layer is needed to prevent the Sn vaporizing.

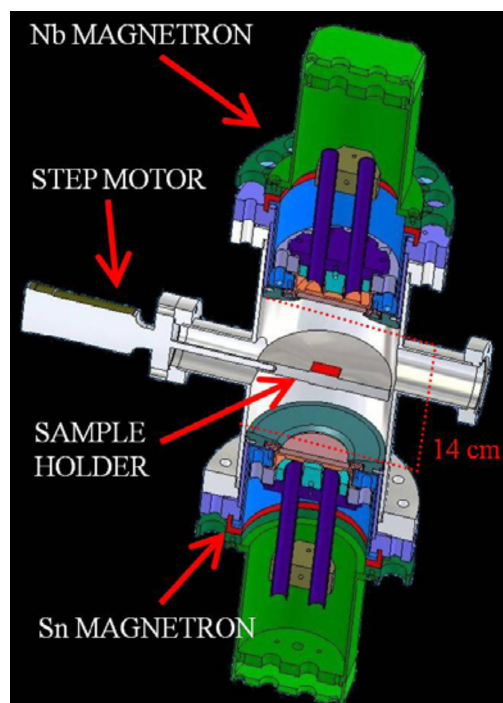

Fig. 3.2 Sketch of the UHV multilayer deposition system

For the deposition of the multilayer in the cylindrical stainless steel vacuum

chamber which is 280 mm high and 100 mm of the diameter, we use two planar balanced magnetrons. The Sn magnetron should be mounted at the bottom of the chamber because of the lower melting point, and the Nb magnetron is mounted at the top of the chamber as shown in Fig. 3.2.

The sample holder is in the centre of the chamber and it is an aluminium disk connected to a rotary feed through. In this way we can rotate the samples, and every 180° rotation we expose the sample to Nb plasma before, and Sn plasma after. The distance between targets and samples is 70 mm and during the sputtering we use Argon as process gas whose pressure is about 10^{-3} mbar. No substrate heating systems were employed.

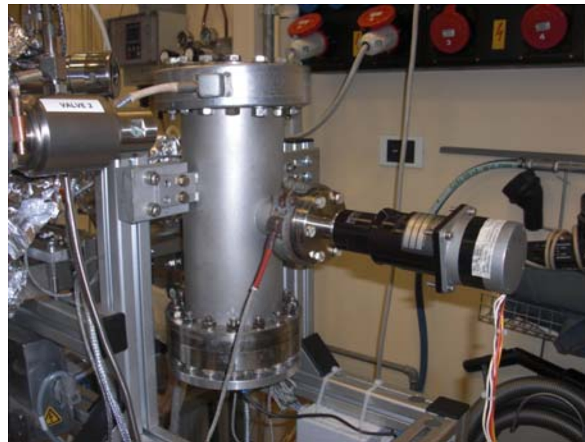

Fig. 3.3 the UHV multilayer deposition chamber

3.2 Deposition on sapphire

The multilayer can be deposited on the sapphire and the Nb sample. Because of the perfect flat of the sapphire surface, all the parameters of the thin film on the sapphire can be measured, such as T_c, RRR, thickness and XRD. On the other side, only T_c and RRR of the thin film on the Nb sample can be measured. So, we first investigate the multilayer deposited on the sapphire.

3.2.1 Deposition parameter

Same with the deposition of Nb thin film on the sapphire, the main parameters of the deposition multilayer are including the sputtering current, the deposition time and the proceeding pressure. In our experiment, we fix the proceeding pressure of $5*10^{-3}$ mbar and the Sn sputtering current of 0.15mA. The deposition time is also fixed. To deposit the buffer layer and over layer, we use the Nb sputtering current of 0.8mA for

1 minute. The time of depositing multilayer is 10 minute. The rotation speed of the sample holder is about 13 second per circle. We only change the Nb sputtering current form 1A to 1.8A. The parameters of each deposition are shown in Table 3.1. Where, ML means multilayer.

Table 3.1 The parameters of multilayer deposition on sapphire

<table>
<tr><td colspan="3">Run</td><td>s1</td><td>s2</td><td>s3</td><td>s4</td><td>s5</td></tr>
<tr><td colspan="3">Total Time(min)</td><td>12</td><td>12</td><td>12</td><td>12</td><td>12</td></tr>
<tr><td colspan="2" rowspan="3">Nb buffer layer</td><td>voltage(V)</td><td>374</td><td>435</td><td>408</td><td>384</td><td>365</td></tr>
<tr><td>current(A)</td><td>0.8</td><td>0.8</td><td>0.8</td><td>0.8</td><td>0.8</td></tr>
<tr><td>time(min)</td><td>1</td><td>1</td><td>1</td><td>1</td><td>1</td></tr>
<tr><td rowspan="5">Multilayer</td><td rowspan="2">Nb</td><td>voltage(V)</td><td>376</td><td>436</td><td>416</td><td>400</td><td>404</td></tr>
<tr><td>current(A)</td><td>1.0</td><td>1.2</td><td>1.4</td><td>1.6</td><td>1.8</td></tr>
<tr><td rowspan="2">Sn</td><td>Voltage(V)</td><td>520</td><td>400</td><td>480</td><td>540</td><td>512</td></tr>
<tr><td>Current(A)</td><td>0.15</td><td>0.15</td><td>0.15</td><td>0.15</td><td>0.15</td></tr>
<tr><td colspan="2">time (min)</td><td>10</td><td>10</td><td>10</td><td>10</td><td>10</td></tr>
<tr><td colspan="2" rowspan="3">Nb over layer</td><td>voltage(V)</td><td>367</td><td>400</td><td>380</td><td>369</td><td>355</td></tr>
<tr><td>current(A)</td><td>0.8</td><td>0.8</td><td>0.8</td><td>0.8</td><td>0.8</td></tr>
<tr><td>time(min)</td><td>1</td><td>1</td><td>1</td><td>1</td><td>1</td></tr>
<tr><td colspan="3">Base pressure(mbar)</td><td>$1.2*10^{-8}$</td><td>$1.5*10^{-8}$</td><td>$4.7*10^{-8}$</td><td>$2.3*10^{-8}$</td><td>$4.9*10^{-8}$</td></tr>
<tr><td colspan="3">Ar Gas pressure(mbar)</td><td>$5*10^{-3}$</td><td>$5*10^{-3}$</td><td>$5*10^{-3}$</td><td>$5*10^{-3}$</td><td>$5*10^{-3}$</td></tr>
</table>

3.2.2 Vacuum annealing

The sample annealing is performed after the deposition for obtaining the A15 of Nb_3Sn. The annealing should first heat the sample and thin film to about 1000°C. During that temperature, the Nb atom and Sn atom diffusion into each other, and then the A15 crystal structure is formed. According to the Fig.3.4, the heating temperature should be higher than 775°C, and the best is from 930°C to 950°C. The heating time should be longer than three hours, and then quench as quickly as possible. If the quenching time is shorter enough, the A15 crystal structure formed during the high temperature is frozen. Otherwise, the A15 crystal structure will be broken at the low temperature.

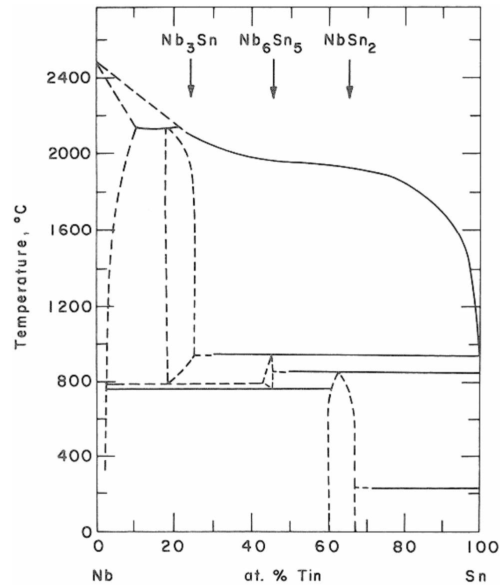

Fig. 3.4 The Niobium-Tin phase diagram

The annealing should be performed in vacuum for good purity and performance. If without vacuum, the gas atom of environment can enter into the thin film or react with the atom of the thin film. So, the base pressure should be also ultra high vacuum, and the baking is also needed. There are two methods of annealing which including the lamp annealing and the inductor annealing.

3.2.2.1 The technique description of lamp annealing

Fig. 3.5 the UHV lamp annealing chamber

The lamp annealing is proceeded in the chamber 4 which is similar with the

chamber 1 and is connected to the same pumping system as shown in Fig. 3.5. A heater, which is composed of an Inconel cup and an infrared lamp in the cup, permits to heat the sample up to 1000°C.

In order to detect the temperature during the annealing, a thermal sensor should be made and mounted in the chamber. The thermal sensor is welded with alumel and chromel on the graphite, and it need to be isolated by a ceramic.

The feed through is needed to isolate the heater and thermal sensor by ceramic. The power is provide by a variac and isolation transformer. The different annealing temperature can be obtained by changing the input voltage of the heater.

Fig. 3.6 Mounting the lamp for annealing heater

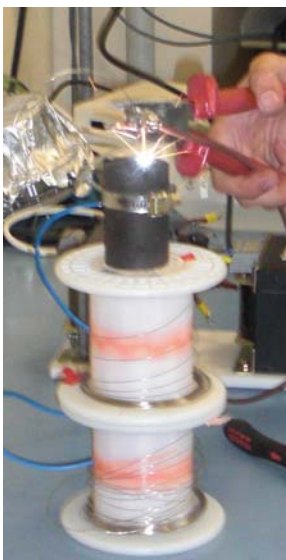

Fig. 3.7 welding the thermal sensor

Fig. 3.8 the thermal sensor after welding

Fig. 3.9 thermal sensor with ceramic isolator

Fig. 3.10 mounting the feed through of heater and thermal sensor

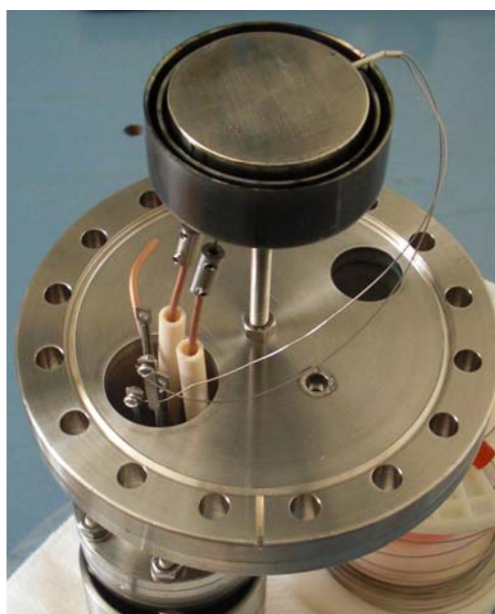

Fig. 3.11 the heater system

3.2.2.2 Analysis result

Ⅰ The thickness measurement

After three hours annealing, we have measured the superconductor parameters of the sapphire sample. The measurement method of thickness is same with that in the Chapter 2. According to the result of measurement, the thickness of each thin film is about 1 um as shown in Table 3.2.

Table 3.2 the thickness of each deposition

Trace number	1	2	3	4	5	average
Run s1(nm)	960	940	930	910	910	930
Run s2(nm)	990	970	960	930	920	950
Run s3(nm)	1050	1030	1030	1030	1040	1040
Run s4(nm)	1050	1040	1080	1110	1180	1090
Run s5(nm)	1140	1140	1180	1180	1240	1180

Ⅱ T_c measurement

The measurement method of T_c and RRR is same with that in the Chapter 2.

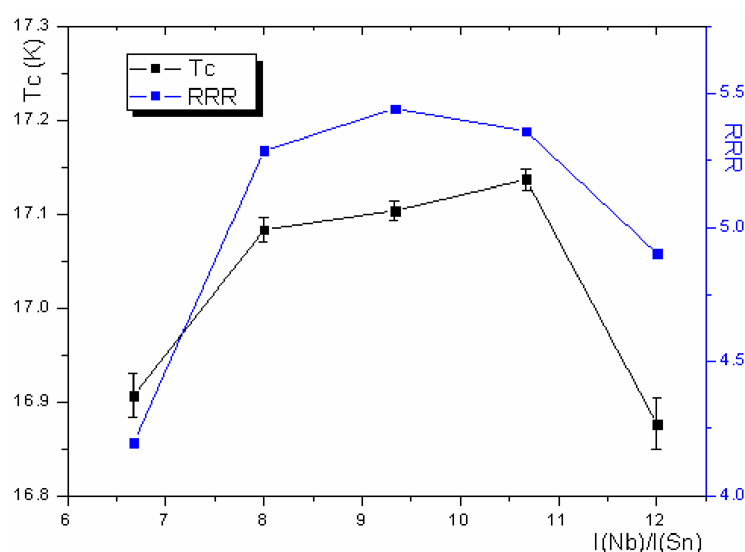

Fig. 3.12 the superconductor parameters of different sample

According to the result of measurement, the T_c is about 17K, and the RRR is about 5. According to the Fig. 3.12, the T_c and RRR decrease at the same time when the ratio of the sputtering current between Nb and Sn is higher or lower than the proper value. This can be explained in the Fig. 3.4 that when the stoichiometric

composition is not proper, other kinds of crystal structure can appear after the annealing, and then the superconductor parameters become worse.

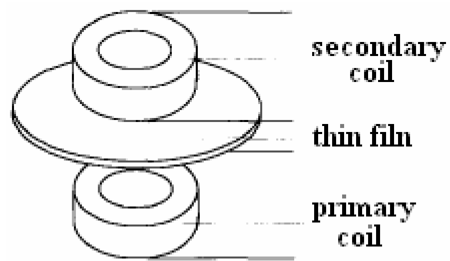

Fig. 3.13 the principle of the inductor T_c measurement

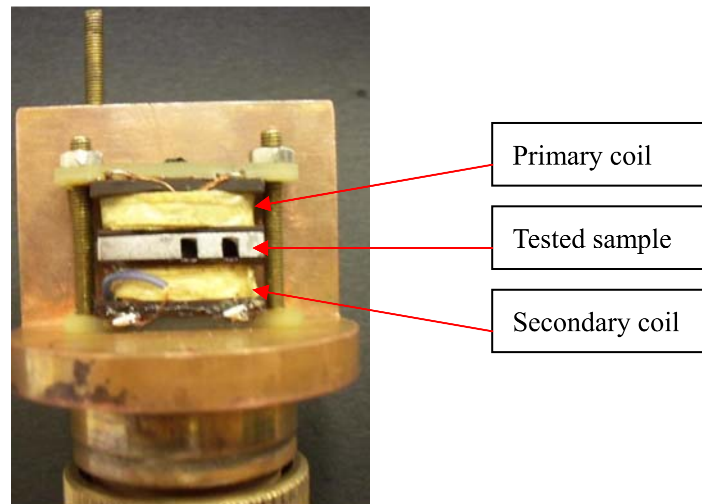

Fig. 3.14 inductor set up for T_c measurement

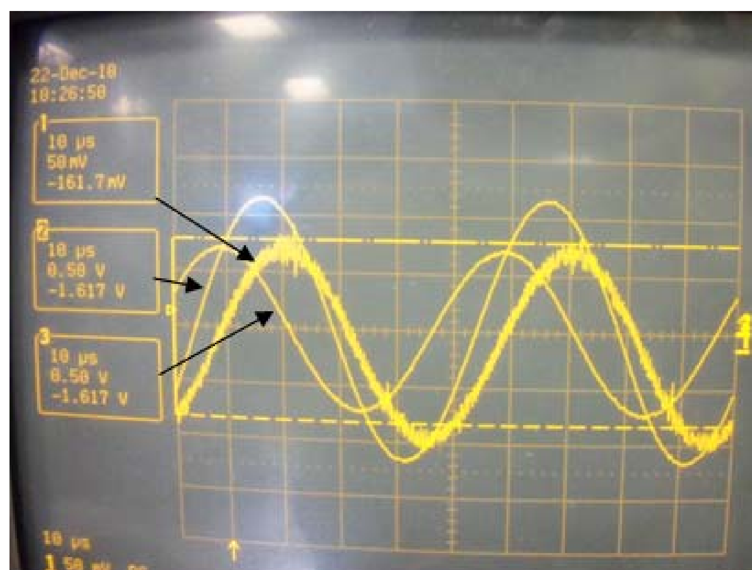

Fig. 3.15 the waveform of the measurement signal

In order to detect the component of the thin film, another method of the inductor T_c measurement should be used as shown in Fig.3.13 [31]. We give a sine signal to the primary coil, and measure the output signal of the secondary coil. In Fig. 3.15, channel 1 is the input signal, channel 2 is the output signal and the channel 3 is the reference signal.

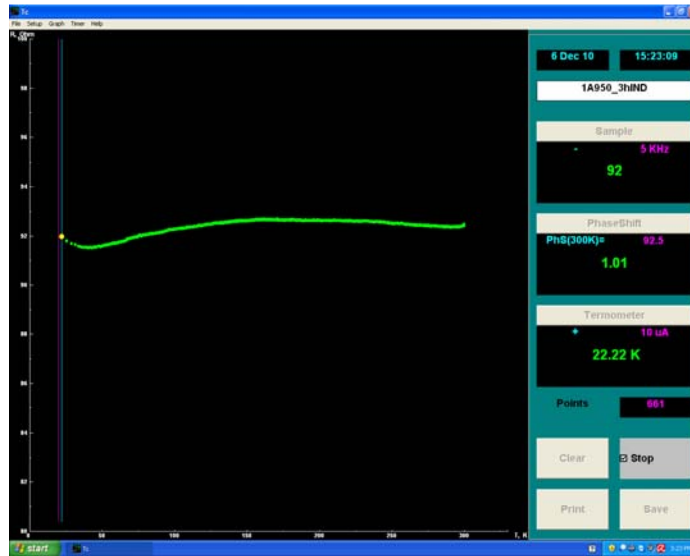

Fig. 3.16 the measurement interface before 20K

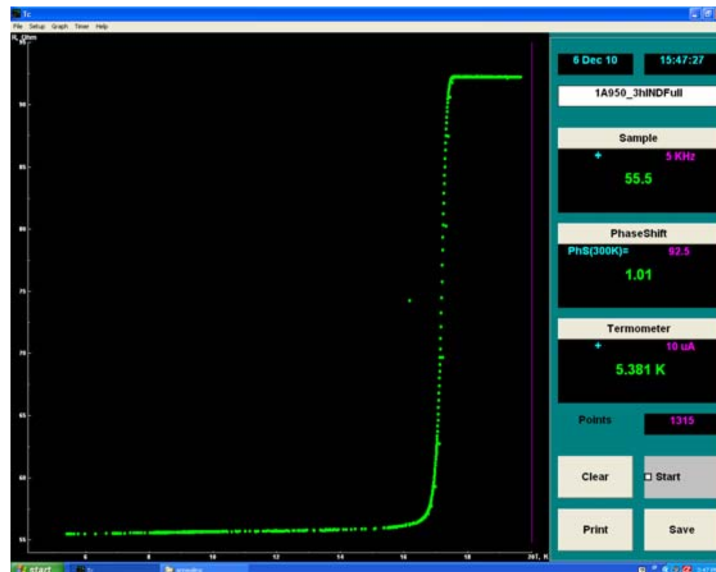

Fig. 3.17 the measurement interface after 20K

Because the thin film is conductor, there is a phase different between the secondary coil and the primary coil. If the thin film is normal conductor, the phase

difference is changed slightly with the temperature as shown in Fig. 3.16. If the thin film transform to superconductor, the phase difference is changed rapidly, as shown in Fig. 3.17. According to the changing of the phase difference, we can measure the T_c as shown in Fig. 3.18, which is similar with that of the resistance measurement method.

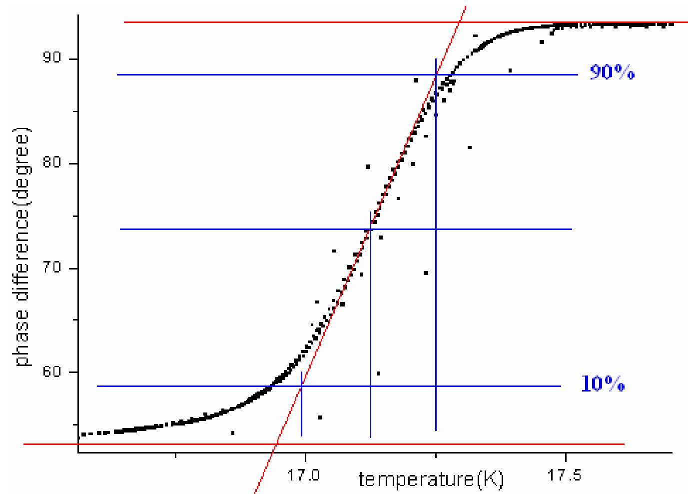

Fig. 3.18 the calculation of the Tc

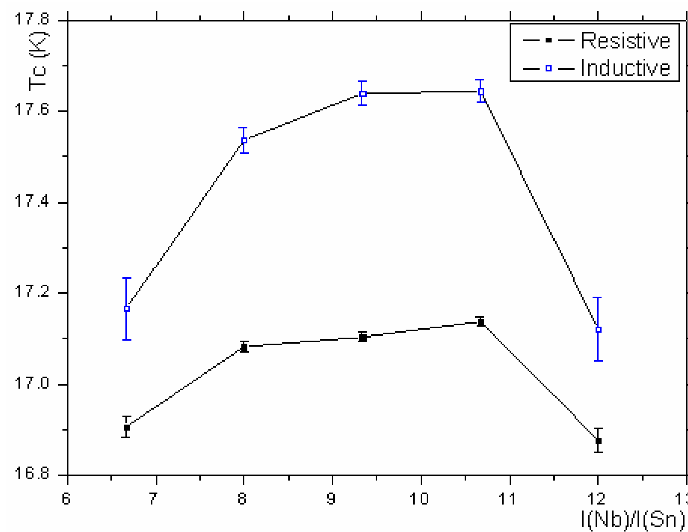

Fig. 3.19 the comparison result of resistive and inductor

The advantage of the inductor method is that it can measure the different T_c of the same thin film. For example, in our experiment, we deposit the Nb and Sn at the same time. If there is some zone of the film composed of pure Nb after the annealing, there will be two step of phase difference changing, where the high temperature of T_c is Nb_3Sn and the lower temperature of T_c is Nb. The disadvantage is that it can not

measure the RRR. So the resistance method can not be replaced by the inductor method completely.

We fix the frequency of the input signal as 20kHz, and the measurement result is shown in Fig. 3.19. Comparing with the result of resistance, the T_c of the measurement by inductor is higher, but the curve shape is similar.

Ⅲ XRD analysis

The crystal structure measured by XRD is shown from Fig. 3.21 to Fig. 3.25. All the marked peaks with black number are the crystal plane of Nb_3Sn. Comparing with the Nb sputtering current from 1.2A to 1.6A, there are several high peak marked with red number as shown in Fig. 3.20 and Fig. 3.24. For the Nb sputtering current of 1.0A, because the abundant of Sn in the thin film, the peak of the Sn crystal plane of 731 appears. The peak of 1' and 2' also exit in the figure from Fig. 3.21 to Fig. 3.23, but its value is small. However, the peak of 1' and 2' is not the crystal plane of Nb, Sn or Nb_3Sn, its meaning need the further investigation.

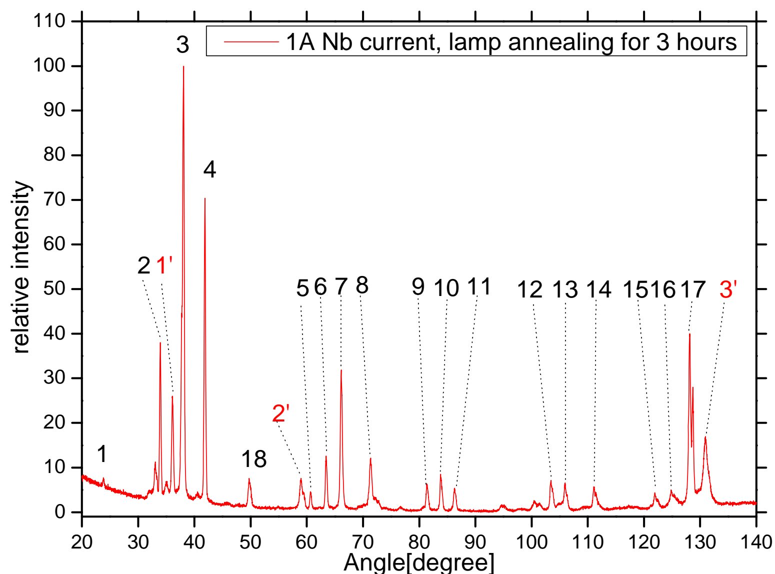

Fig. 3.20 the XRD result of Run s1

Table 3.3 the description of the peaks of Run s1

number	1	2	3	4	5	6	7	8	9	10	11	12	13	14	15	16	17	18
angle	23.81	33.93	38.07	41.87	60.65	63.43	66.13	71.37	81.33	83.81	86.31	103.45	105.97	111.07	121.91	124.83	128.13	49.77
plane	110	200	210	211	222	320	321	400	420	421	332	520	521	440	600	610	611	220
number	1'	2'	3'															
angle	36.11	59.01	130.93															
plane			Sn731															

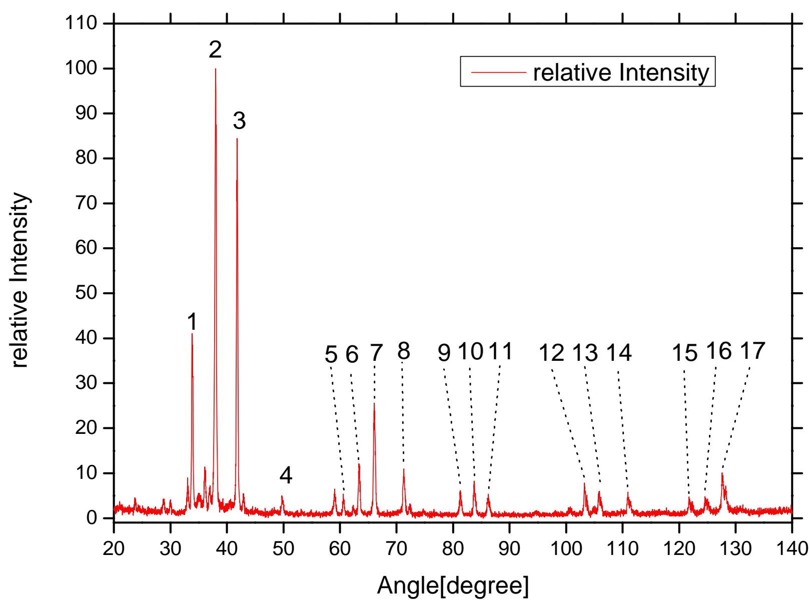

Fig. 3.21 the XRD result of Run s2

Table 3.4 the description of the peaks of Run s2

number	1	2	3	4	5	6	7	8	9	10	11	12	13	14	15	16	17
angle	33.85	38.1	41.81	49.73	60.57	63.33	66.07	71.29	81.27	83.73	86.23	103.27	105.89	110.97	121.77	124.57	127.59
plane	200	210	211	220	222	320	321	400	420	421	332	520	521	440	600	610	611

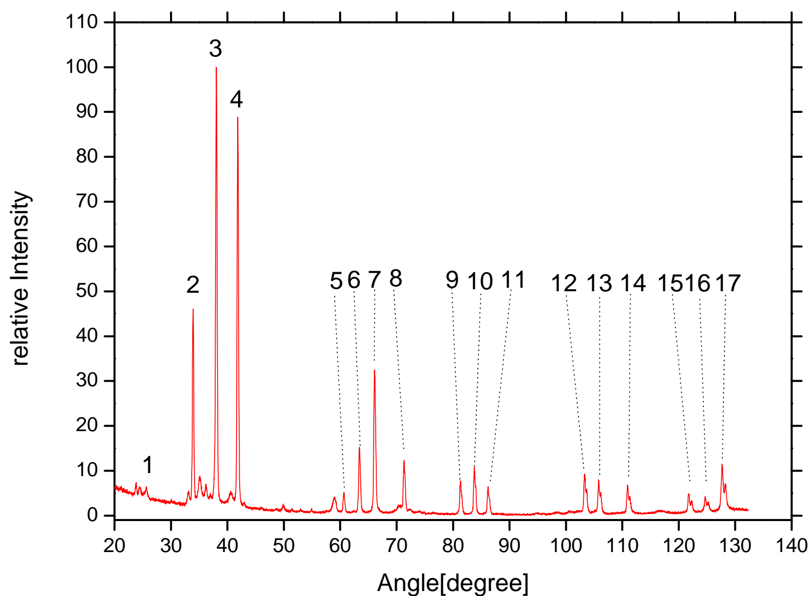

Fig. 3.22 the XRD result of Run s3

Table 3.5 the description of the peaks of Run s3

number	1	2	3	4	5	6	7	8	9	10	11	12	13	14	15	16	17
angle	23.77	33.95	38.07	41.83	60.65	63.43	66.09	71.35	81.41	83.77	86.17	103.39	105.83	110.97	121.77	124.73	127.71
plane	110	200	210	211	222	320	321	400	420	421	332	520	521	440	600	610	611

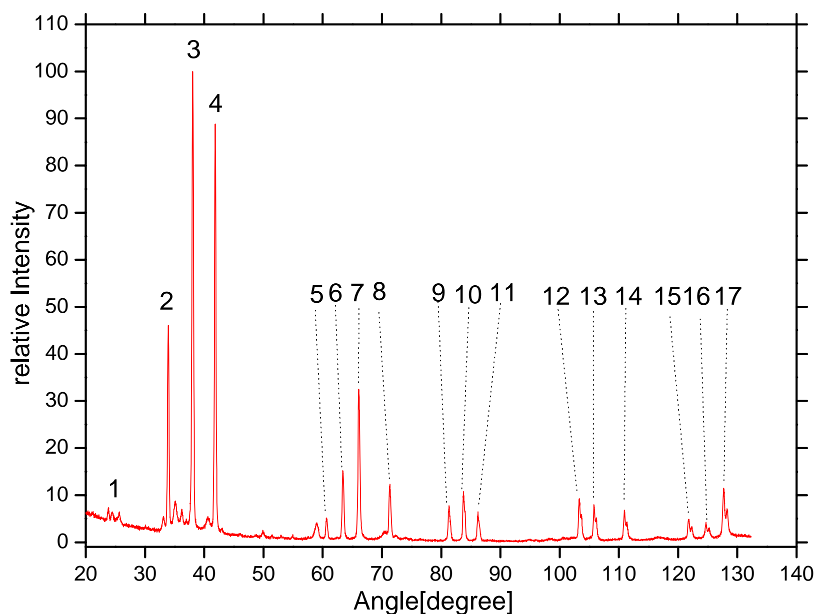

Fig. 3.23 the XRD result of Run s4

Table 3.6 the description of the peaks of Run s4

number	1	2	3	4	5	6	7	8	9	10	11	12	13	14	15	16	17
angle	23.85	33.91	38.07	41.85	60.65	63.39	66.07	71.33	81.31	83.77	86.19	103.31	105.79	110.91	121.79	124.69	127.69
plane	110	200	210	211	222	320	321	400	420	421	332	520	521	440	600	610	611

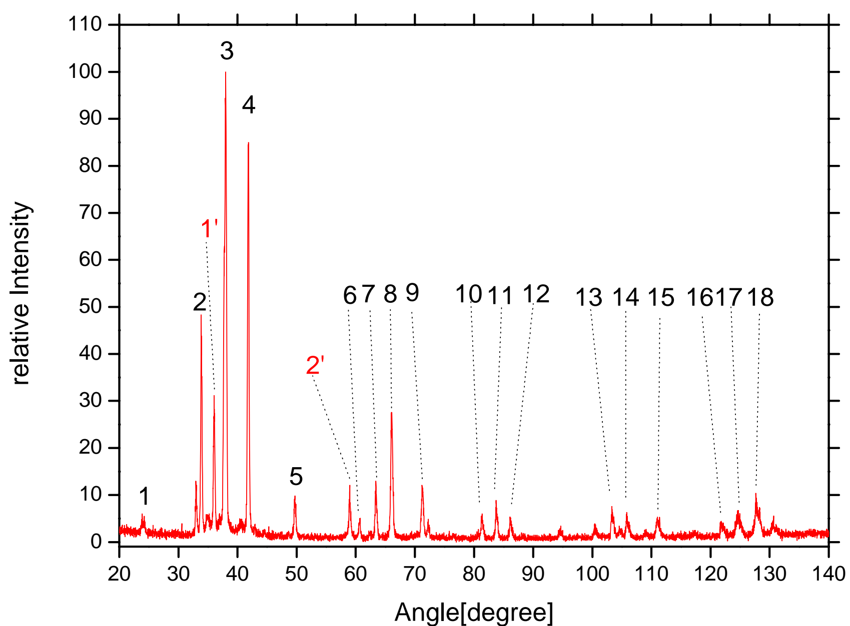

Fig. 3.24 the XRD result of Run s5

Table 3.7 the description of the peaks of Run s5

number	1	2	3	4	5	6	7	8	9	10	11	12	13	14	15	16	17	18
angle	23.87	33.85	38.01	41.83	49.71	60.65	63.39	66.03	71.21	81.37	83.73	86.11	103.31	105.85	111.01	121.73	124.73	127.69
plane	110	200	210	211	220	222	320	321	400	420	421	332	520	521	440	600	610	611
number	1'	2'																
angle	36.03	58.99																
plane																		

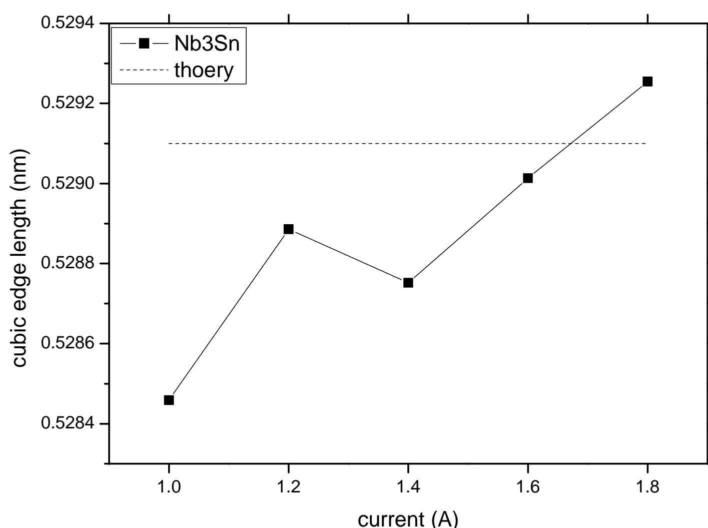

Fig.3.25 the cubic edge length versus Nb sputtering current

Using the same method of 2.3.3.3 section, we can obtain the cubic edge length of each sample. According to Fig.3.25, the cubic edge length increases with the Nb sputtering current increasing, except the point of 1.4A.

3.3 Deposition on Nb sample

If we fabricate the accelerator cavity with thin film, the thin film should be deposited on substrate, which including the Nb and copper. The advantage of the Nb substrate is that Nb is superconductor, which means that when the part zone of the thin film is not the superconductor, the Nb is still the superconductor which make sure of that the whole accelerator cavity is superconductor. But the disadvantage is that the thermal conductor of the Nb is poor. The advantage of the copper substrate is that the thermal conductor and the mechanical property are very good. The good thermal conductor can quickly transfer the heat produced by the microwave in the thin film, which can reduce the thermal unstable of the superconductor because that if the heat can not transfer in time, the temperature of some zone of the thin film will increase and higher than T_c. The good mechanical property can reduce the detuning of the

frequency of the cavity which is induced by the Lorentz force acting on the superconductor by the microwave. But the copper is not superconductor.

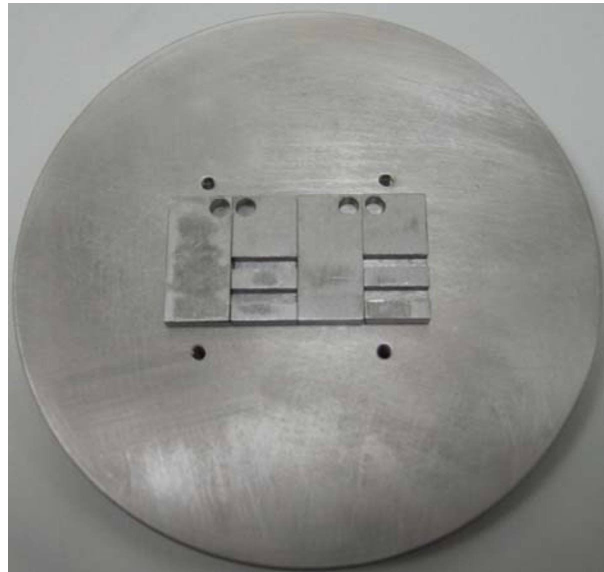

Fig. 3.26 the Nb sample and its holder

The Nb sample and its holder before and after mounting are shown in Fig3.26 and Fig.3.27. The Nb sample is 2cm length, 1cm width and 3mm thickness with two grooves of 2mm width. Before the deposition, the Nb sample is preceded with the buffer chemical polish (BCP) for 5 minute. The sputtering and the depositing system are same with that of sapphire sample.

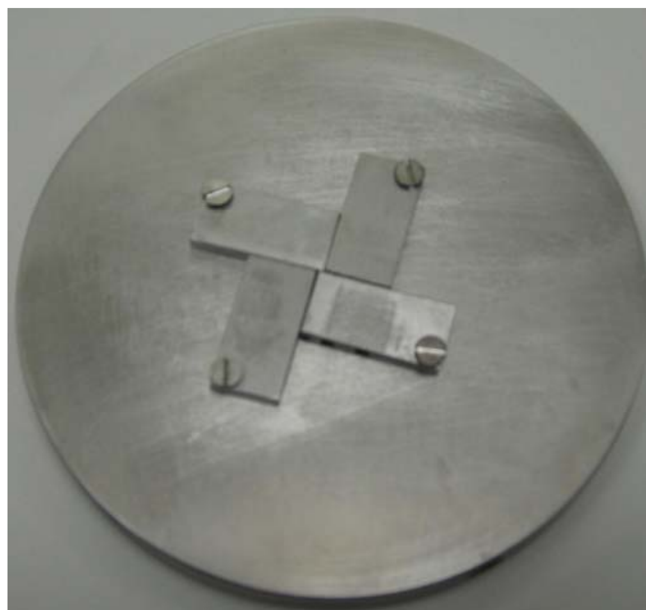

Fig. 3.27 fixing the sample on its holder

3.3.1 Deposition parameter

The deposition parameters of the multilayer of thin film on the Nb sample are the same with that on the sapphire sample, which is shown in Table 3.8.

Table 3.8 The parameters of multilayer deposition on Nb

<table>
<tr><td colspan="3">Run</td><td>N1</td><td>N2</td><td>N3</td><td>N4</td><td>N5</td></tr>
<tr><td colspan="3">Total Time(min)</td><td>12</td><td>12</td><td>12</td><td>12</td><td>12</td></tr>
<tr><td colspan="2" rowspan="3">Nb buffer layer</td><td>voltage(V)</td><td>343</td><td>338</td><td>341</td><td>356</td><td>330</td></tr>
<tr><td>current(A)</td><td>0.8</td><td>0.8</td><td>0.8</td><td>0.8</td><td>0.8</td></tr>
<tr><td>time(min)</td><td>1</td><td>1</td><td>1</td><td>1</td><td>1</td></tr>
<tr><td rowspan="5">multilayer</td><td rowspan="2">Nb</td><td>voltage(V)</td><td>344</td><td>358</td><td>360</td><td>375</td><td>372</td></tr>
<tr><td>current(A)</td><td>1.0</td><td>1.2</td><td>1.4</td><td>1.6</td><td>1.8</td></tr>
<tr><td rowspan="2">Sn</td><td>Voltage(V)</td><td>493</td><td>497</td><td>521</td><td>506</td><td>489</td></tr>
<tr><td>Current(A)</td><td>0.15</td><td>0.15</td><td>0.15</td><td>0.15</td><td>0.15</td></tr>
<tr><td colspan="2">time (min)</td><td>10</td><td>10</td><td>10</td><td>10</td><td>10</td></tr>
<tr><td colspan="2" rowspan="3">Nb over layer</td><td>voltage(V)</td><td>121*</td><td>334</td><td>331</td><td>332</td><td>323</td></tr>
<tr><td>current(A)</td><td>0.8</td><td>0.8</td><td>0.8</td><td>0.8</td><td>0.8</td></tr>
<tr><td>time(min)</td><td>1</td><td>1</td><td>1</td><td>1</td><td>1</td></tr>
<tr><td colspan="3">Ar Gas pressure(mbar)</td><td>$5*10^{-3}$</td><td>$5*10^{-3}$</td><td>$5*10^{-3}$</td><td>$5*10^{-3}$</td><td>$5*10^{-3}$</td></tr>
<tr><td colspan="3">Base pressure(mbar)</td><td>$4.3*10^{-8}$</td><td>$4.8*10^{-8}$</td><td>$1.8*10^{-8}$</td><td>$3.0*10^{-8}$</td><td>$1.5*10^{-8}$</td></tr>
</table>

* The leakage water induce the short circuit and low output voltage

3.3.2 Annealing with inductor

Annealing with lamp needs long time to increase the temperature. The ramp of the temperature is very steep when the inductor is used. The inductor annealing needs to input the AC current into the coil. As shown in Fig. 3.28. The coil will induce the electromagnetic field in the vacuum chamber space. When we put the sample or the cavity, the eddy current will be induced in the metal and the eddy current will heat the metal quickly.

Fig. 3.28 the inductor coil

During the annealing, the temperature is measured by the pyrometer. The pyrometer measures the temperature of the annealing sample through the glass window as shown in Fig. 3.30. Because the spectrum of the photon emitted form the sample at the different temperature is different, we can measure the temperature by the spectrum.

The maximum of the input power of the inductor is about 10KW, and we fix the frequency of the input AC current at 80KHz.

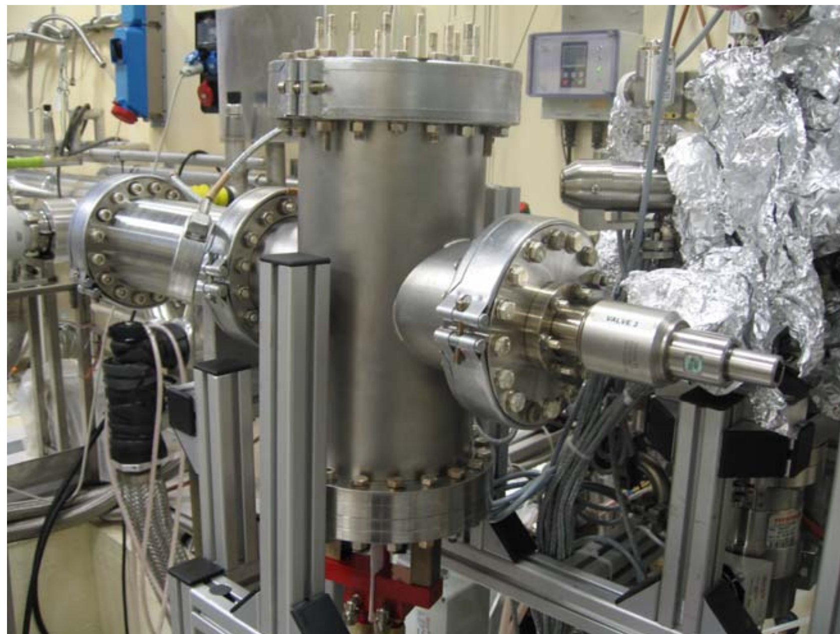

Fig.3.29 the inductor annealing chamber

Fig. 3.30 Pyrometer

Fig. 3.31 measuring the temperature of the sample during annealing

Only the inductor annealing is used for obtaining the Nb_3Sn thin film on Nb sample. The sample is fixed by Nb wire as shown in Fig.3.32. The temperature of the sample is about 1000℃ during the annealing.

Fig. 3.32 fixing the sample with Nb wire

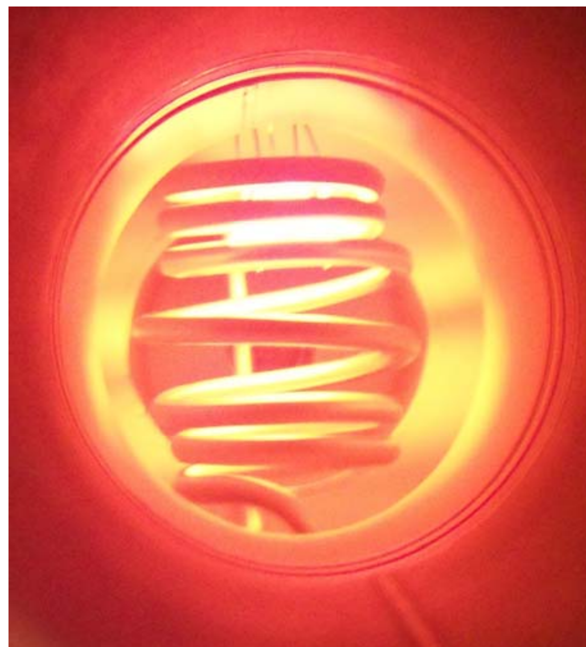

Fig. 3.33 heating the sample by the inductor

3.3.3 Analysis result

3.3.3.1 Tc measurement

Because the thin film is deposited on the Nb sample and the resistance of the sample is too small to measure it, we have to use the inductor T_c measurement. Three

transition temperatures are found during the measurement as shown in Fig. 3.34.

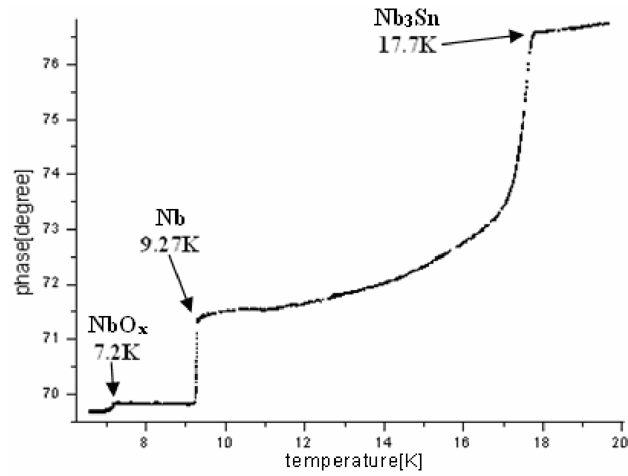

Fig. 3.34 three transition temperature of the T_c curve

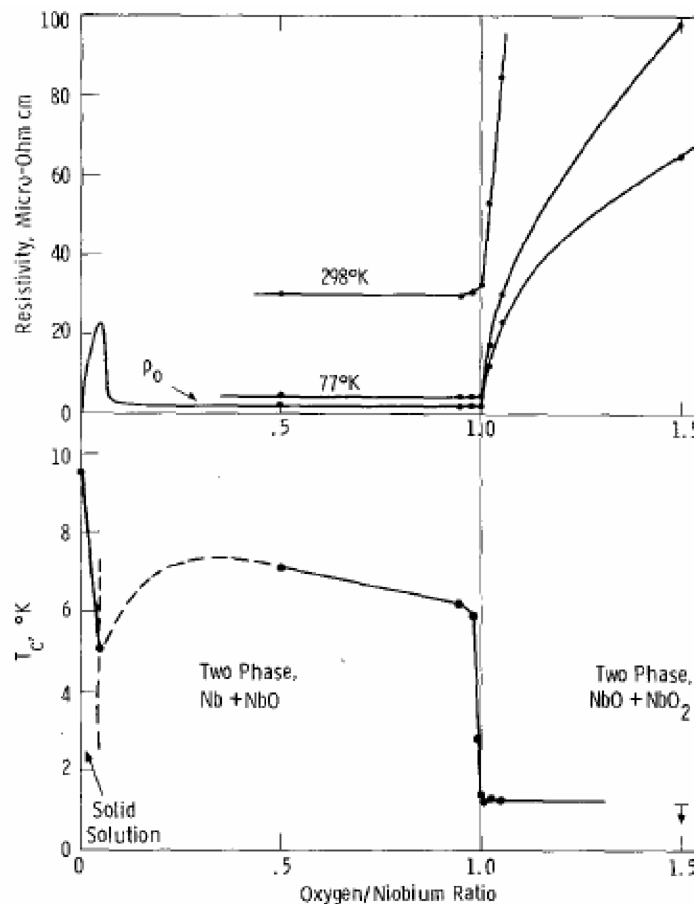

Fig. 3.35 Electrical resistivity and superconducting critical temperature as a function of composition; as-cast alloys of niobium and oxygen.

It is no doubt that the first transition temperature is the T_c of Nb_3Sn and the

second transition temperature is the T_c of Nb. The third transition temperature is impossible to be the T_c of Nb_5Sn_6 or $NbSn_2$, because the Tc of them is no more than 3K [32]. Also, according to the Fig. 3.37 and Fig.3.41, the third transition temperature is almost invariable with the changing of the Nb sputtering current, which means that the third transition temperature is also impossible to be the T_c of the mixture of the Nb_5Sn_6, $NbSn_2$ and Nb, because if there is the mixture, the T_c should be change with the different composition of them.

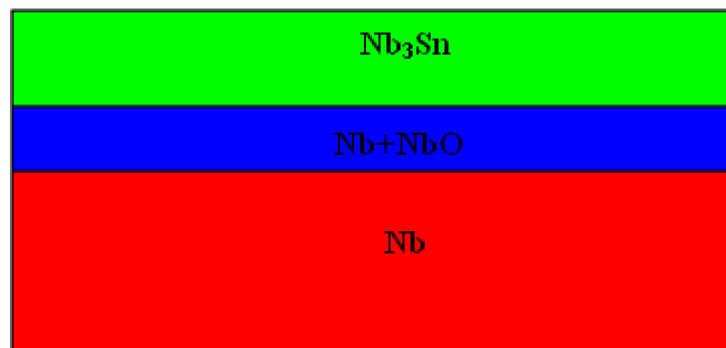

Fig. 3.36 the possible structure of the sample

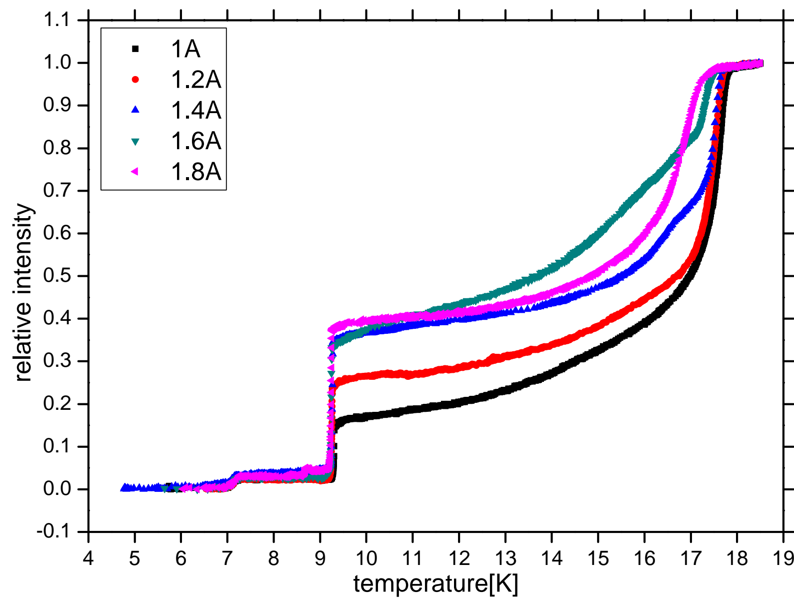

Fig. 3.37 the transition temperature curve of the sample annealed with 5 minutes

According to the Fig. 3.35 [33], the third transition temperature should be the T_c of NbO_x. When the ratio of Oxygen and Nb is greater than 1.0, the T_c should be about 1.38K. According to the third transition temperature of 7.2K given by the experiment,

the ratio of Oxygen and Nb should be about 0.5, which means that there should be a layer of the mixture of Nb and NbO. Because the Nb_3Sn cover the bulk Nb and have the higher T_c, there is some shielding effect during the temperature between 9.2K to 17K. The shielding effect is different with the Nb sputtering current, but its ruler is not clear.

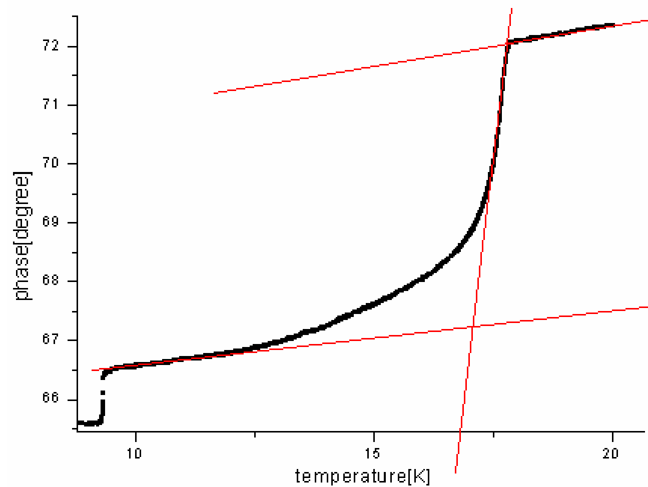

Fig. 3.38 the T_c calculation of Nb_3Sn

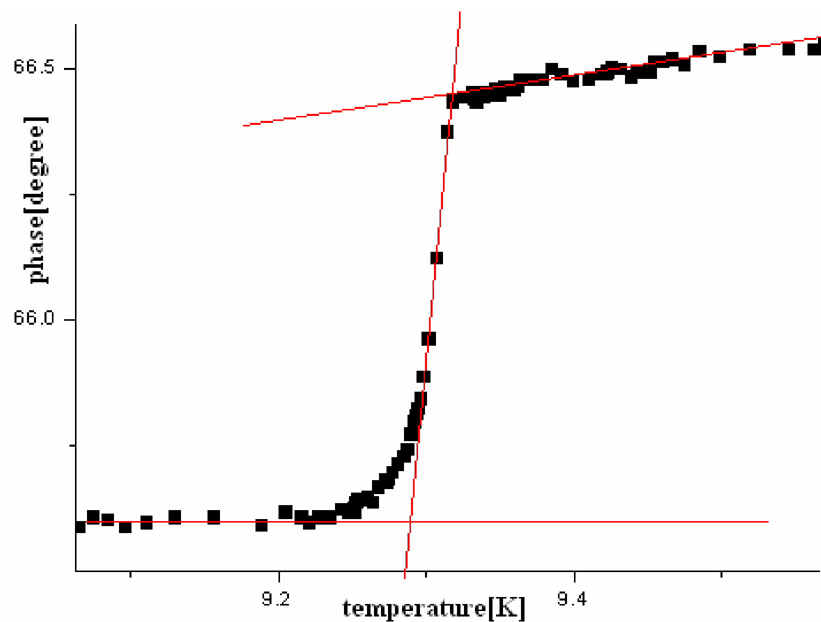

Fig. 3.39 the T_c calculation of Nb

The possible structure of the sample could be like as the Fig. 3.36. Because the NbO has a large ratio and the Nb_3Sn thin film deposited on the sapphire have no the third transition temperature, it should not come from the Nb_3Sn thin film, and the only

source is the bulk Nb sample. Although the sample is preceded with BCP, the NbO coming from the oxidation with the atmosphere for a long time can not be got rid of with a short time of 5 minute. So we need to test the more BCP time.

All the other temperature transition curves are shown in Fig. 3.37. Among these curves, the best is the curve of 1A Nb sputtering current. The calculation method of the three critical temperatures is shown from Fig. 3.38 to Fig. 3.40.

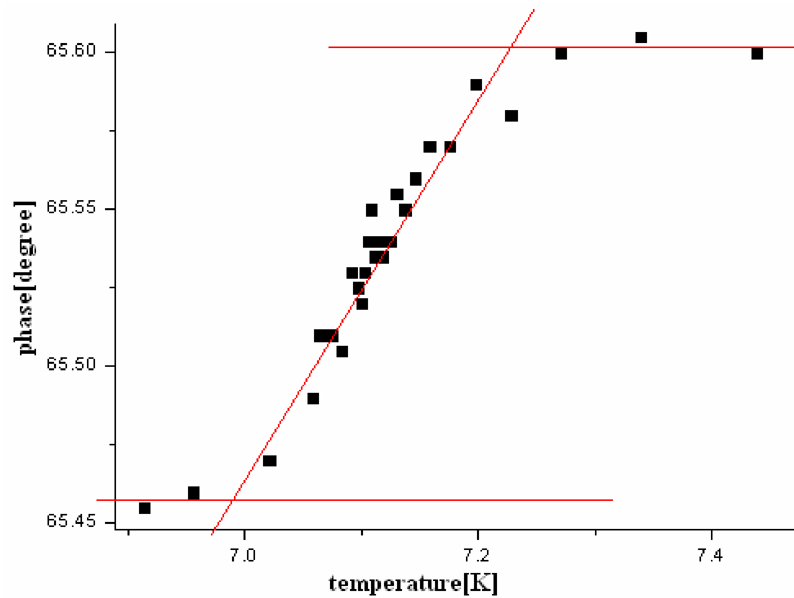

Fig. 3.40 the T_c calculation of NbO_x

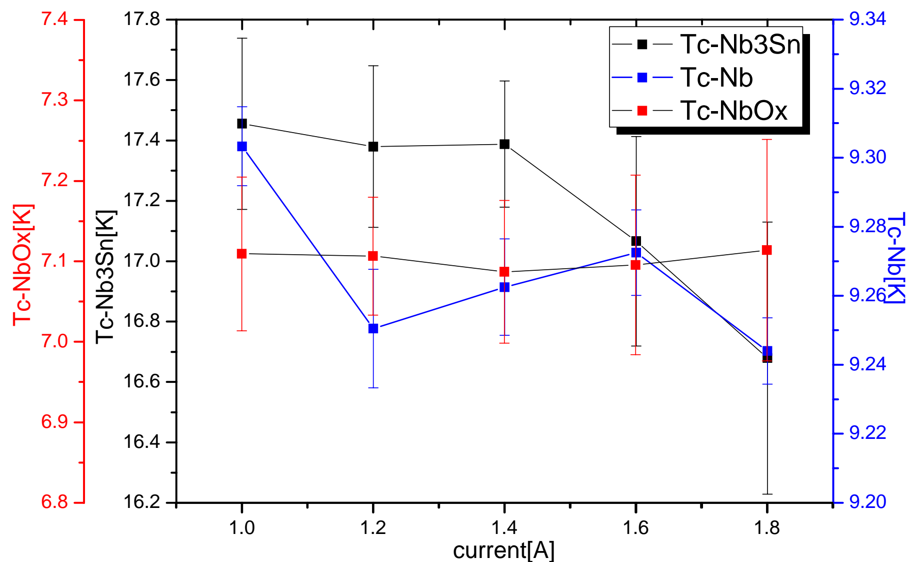

Fig. 3.41 the Tc calculation result of the sample annealing with 5 minutes

The T_c calculation result of the sample annealing with 5 minutes is shown in Fig. 3.41, which show that the T_c of 1A is the highest temperature.

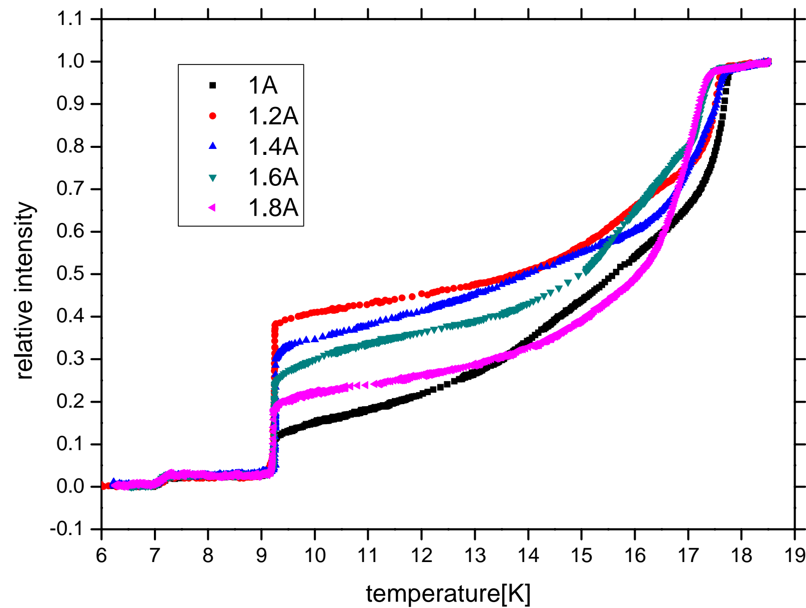

Fig. 3.42 the transition temperature curve of the sample annealed with 10 minutes

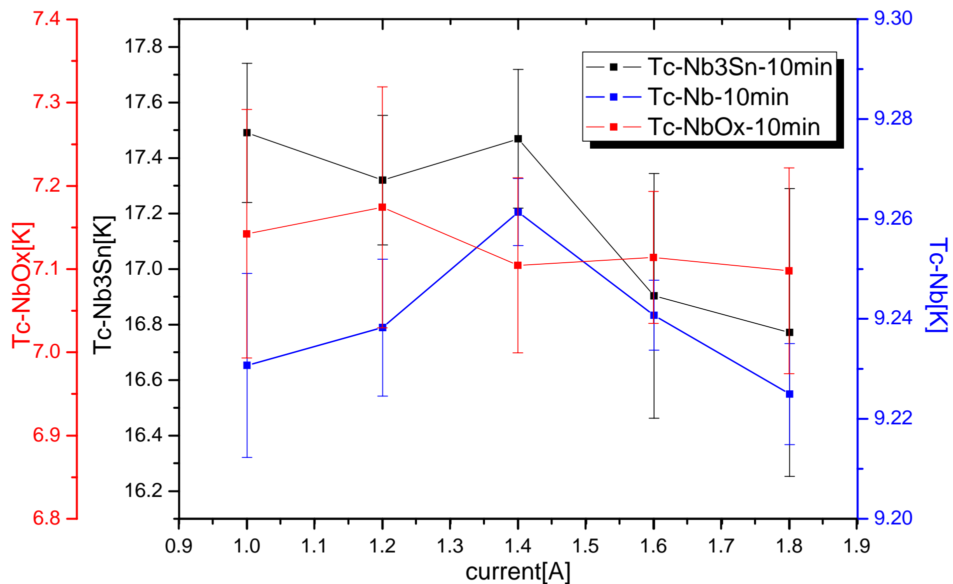

Fig. 3.43 the Tc calculation result of the sample annealing with 10 minutes

We anneal the second sample of each run for 10 minutes. The temperature transition of 1A is also the best as shown in Fig. 3.42. The reason of the better result

of 1A in the Fig. 3.37 and Fig. 3.42 may be that the thin film is without the Nb cover layer. About the other curve, the shielding effect is clear compare with the Fig. 3.37, which is that the higher Nb sputtering current, the more shielding effect, but the higher Nb sputtering current the lower transition temperature of Nb_3Sn.

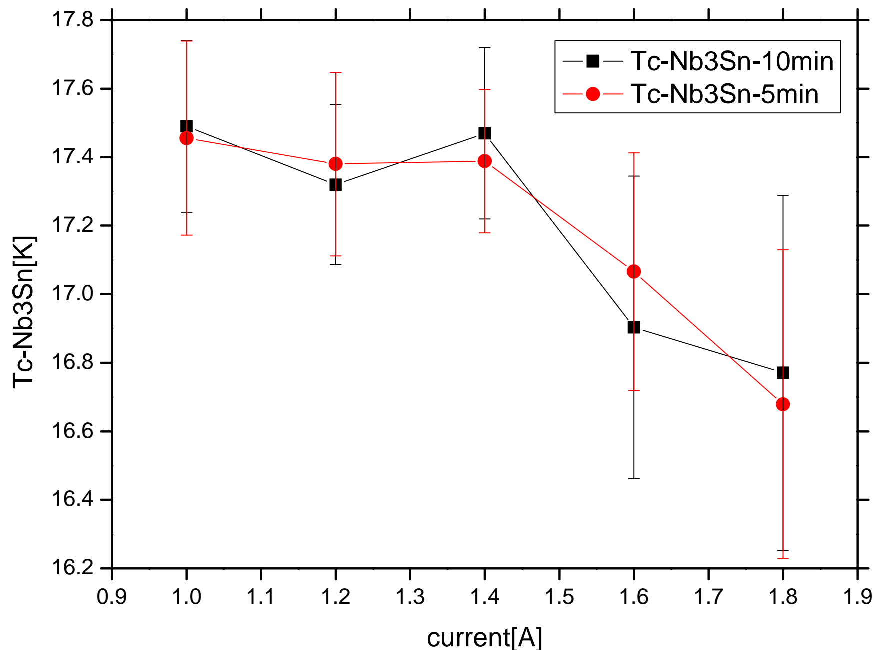

Fig. 3.44 comparing the Nb_3Sn Tc with the different annealing time

The T_c of Nb_3Sn, Nb and NbO_x of the sample annealed for 10 minutes are shown in Fig. 3.43. The T_c of NbO_x and Nb should depend on the property of the bulk Nb, which is same with the sample annealed for 5 minutes. The Tc of Nb_3Sn should depend on the parameters of the sputtering and the annealing. However, the parameter of annealing has little effect on the T_c as shown in Fig.3.44. Comparing with Fig.3.19, the T_c of 1A should be lower than that of 1.2A. The reason of the abnormal result may be the absentation over layer of 1A sample.

3.3.3.2 XRD analysis

The XRD analysis method is same with that in Chapter 2. We do the annealing experiment for 5 minutes and 10 minutes.

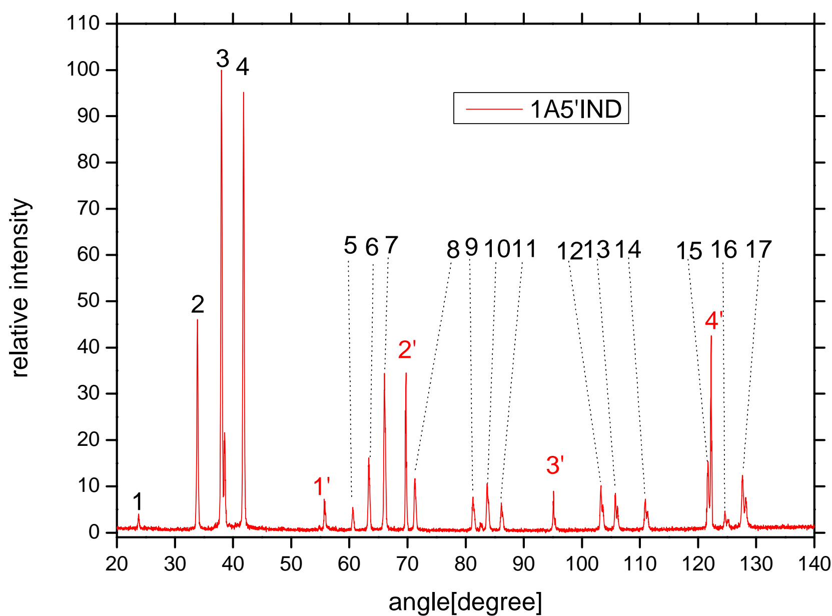

Fig. 3.45 the XRD result of Nb sputtering current 1A with annealing for 5 minutes

Table 3.9 the description of the peaks of 1A with annealing for 5 minutes

number	1	2	3	4	5	6	7	8	9	10	11	12	13	14	15	16	17
angle	23.77	33.87	38.01	41.79	60.59	63.35	66.05	71.27	81.27	83.69	86.13	103.29	105.79	110.93	121.69	124.59	127.61
plane	110	200	210	211	222	320	321	400	420	421	332	520	521	440	600	610	611
number	1'	2'	3'	4'													
angle	55.67	69.75	95.15	122.3													
plane	Nb200	Nb211	Nb310	Nb321													

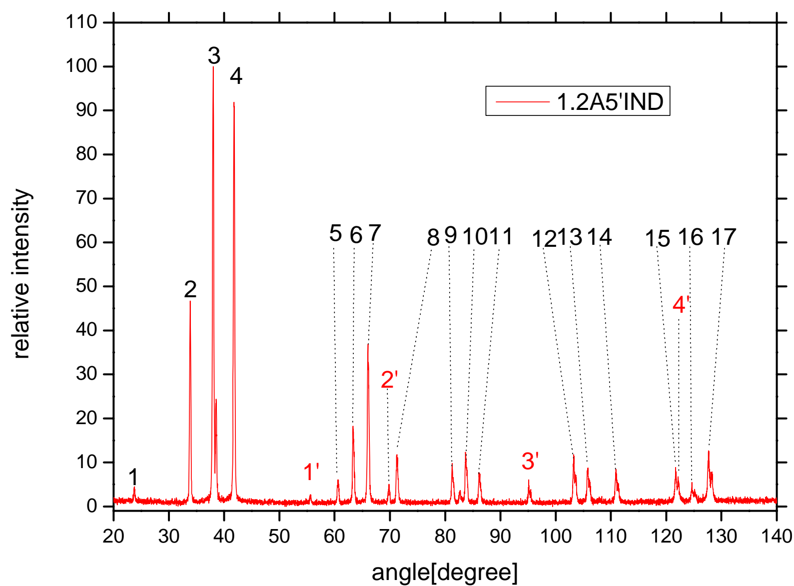

Fig. 3.46 the XRD result of Nb sputtering current 1.2A with annealing for 5 minutes

Table 3.10 the description of the peaks of 1.2A with annealing for 5 minutes

number	1	2	3	4	5	6	7	8	9	10	11	12	13	14	15	16	17
angle	23.79	33.89	38.03	41.79	60.57	63.31	66.03	71.27	81.25	83.69	86.11	103.23	105.75	110.91	121.71	124.63	127.65
plane	110	200	210	211	222	320	321	400	420	421	332	520	521	440	600	610	611
number	1'	2'	3'	4'													
angle	55.63	69.87	95.13	122.19													
plane	Nb200	Nb211	Nb310	Nb321													

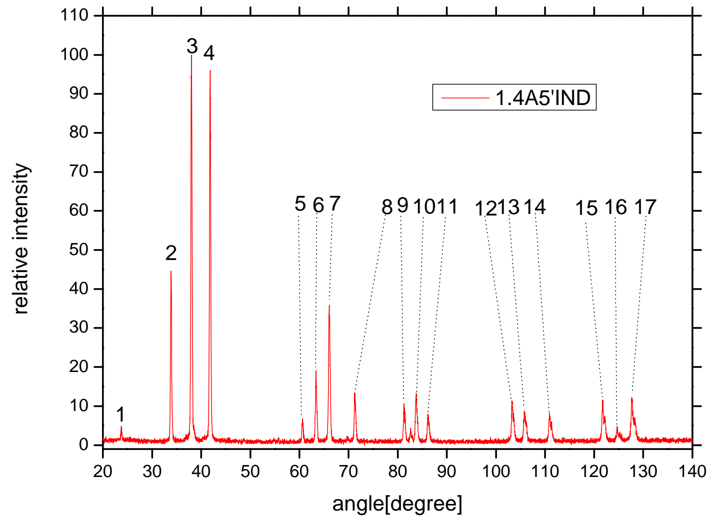

Fig. 3.47 the XRD result of Nb sputtering current 1.4A with annealing for 5 minutes

Table 3.11 the description of the peaks of 1.4A with annealing for 5 minutes

number	1	2	3	4	5	6	7	8	9	10	11	12	13	14	15	16	17
angle	23.73	33.87	38.05	41.83	60.61	63.35	66.09	71.27	81.29	83.79	86.19	103.27	105.77	110.91	121.77	124.71	127.65
plane	110	200	210	211	222	320	321	400	420	421	332	520	521	440	600	610	611

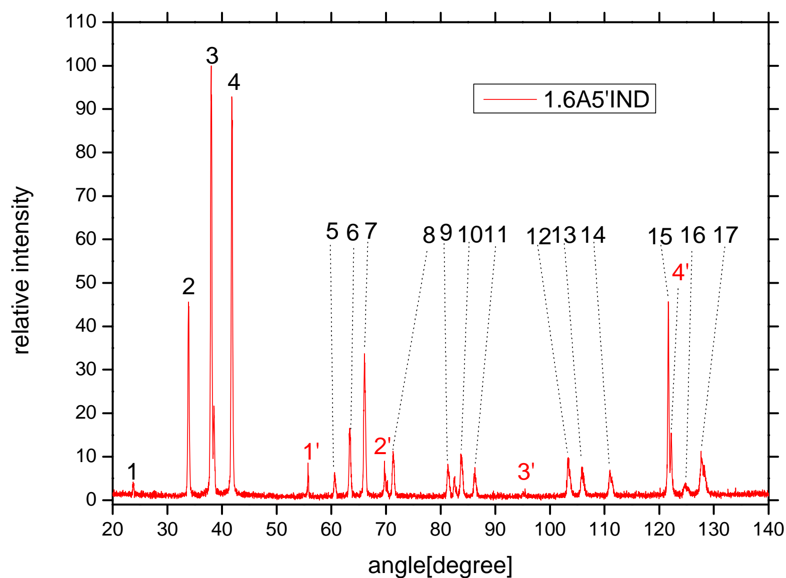

Fig. 3.48 the XRD result of Nb sputtering current 1.6A with annealing for 5 minutes

Table 3.12 the description of the peaks of 1.6A with annealing for 5 minutes

number	1	2	3	4	5	6	7	8	9	10	11	12	13	14	15	16	17
angle	23.75	33.87	38.03	41.81	60.61	63.39	66.07	71.31	81.33	83.69	86.25	103.35	105.89	110.97	121.67	124.77	127.65
plane	110	200	210	211	222	320	321	400	420	421	332	520	521	440	600	610	611
number	1'	2'	3'	4'													
angle	55.73	69.75	95.45	122.2													
plane	Nb200	Nb211	Nb310	Nb321													

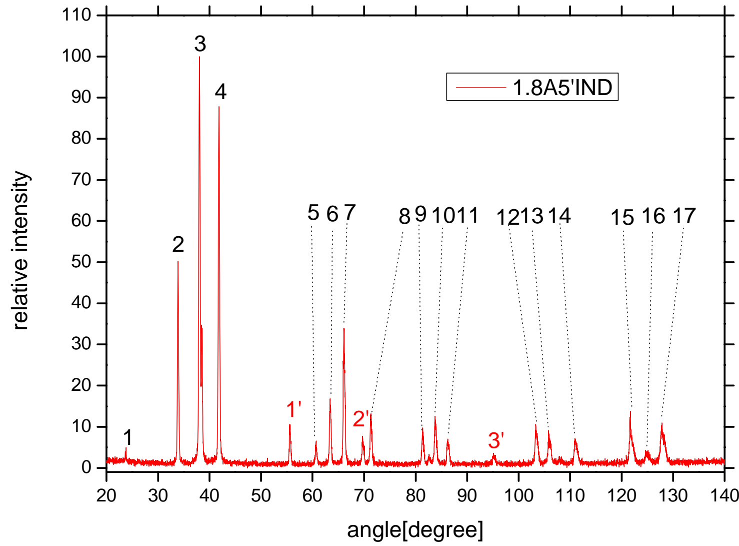

Fig. 3.49 the XRD result of Nb sputtering current 1.8A with annealing for 5 minutes

Table 3.13 the description of the peaks of 1.8A with annealing for 5 minutes

number	1	2	3	4	5	6	7	8	9	10	11	12	13	14	15	16	17
angle	23.79	33.89	38.05	41.83	60.69	63.43	66.07	71.35	81.37	83.79	86.25	103.33	105.83	110.91	121.71	124.63	127.83
plane	110	200	210	211	222	320	321	400	420	421	332	520	521	440	600	610	611
number	1'	2'	3'														
angle	55.63	69.71	95.11														
plane	Nb200	Nb211	Nb310														

According to the XRD analysis of 5 minutes annealing example, there is no Sn crystal plane in all of the samples. But there is Nb crystal plane except the sample with the Nb sputtering current of 1.4A. Only the sample with the Nb sputtering current of 1.0A has the great peak of the Nb crystal plane, which reason is that the thin film is not covered with cover layer. The marked peaks with black number are the crystal plane of Nb_3Sn, and that with red number is the crystal plane of Nb.

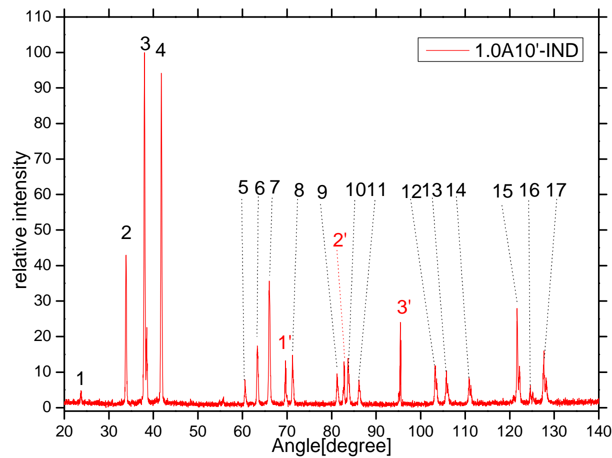

Fig. 3.50 the XRD result of Nb sputtering current 1.0A with annealing for 10 minutes

Table 3.14 the description of the peaks of 1.0A with annealing for 10 minutes

number	1	2	3	4	5	6	7	8	9	10	11	12	13	14	15	16	17
angle	23.73	33.87	38.01	41.79	60.55	63.33	66.01	71.23	81.25	83.68	86.14	103.26	105.78	110.91	121.67	124.61	127.64
plane	110	200	210	211	222	320	321	400	420	421	332	520	521	440	600	610	611
number	1'	2'	3'														
angle	69.65	82.81	95.45														
plane	Nb211	Nb220	Nb310														

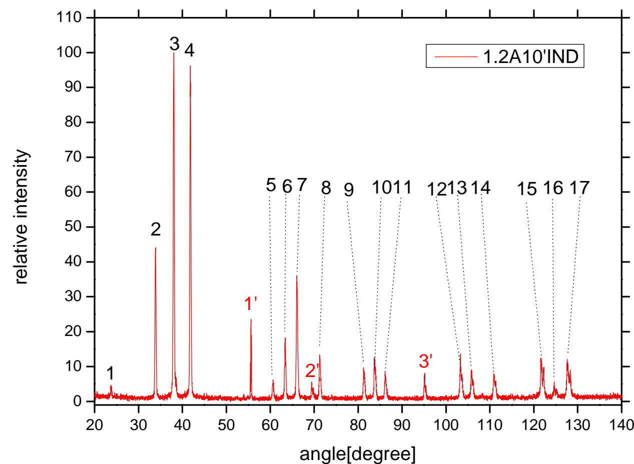

Fig. 3.51 the XRD result of Nb sputtering current 1.2A with annealing for 10 minutes

Table 3.15 the description of the peaks of 1.2A with annealing for 10 minutes

number	1	2	3	4	5	6	7	8	9	10	11	12	13	14	15	16	17
angle	23.74	33.84	37.99	41.79	60.58	63.34	66.03	71.25	81.27	83.73	86.16	103.29	105.8	110.92	121.7	124.64	127.63
plane	110	200	210	211	222	320	321	400	420	421	332	520	521	440	600	610	611
number	1'	2'	3'														
angle	55.59	69.45	95.17														
plane	Nb200	Nb211	Nb310														

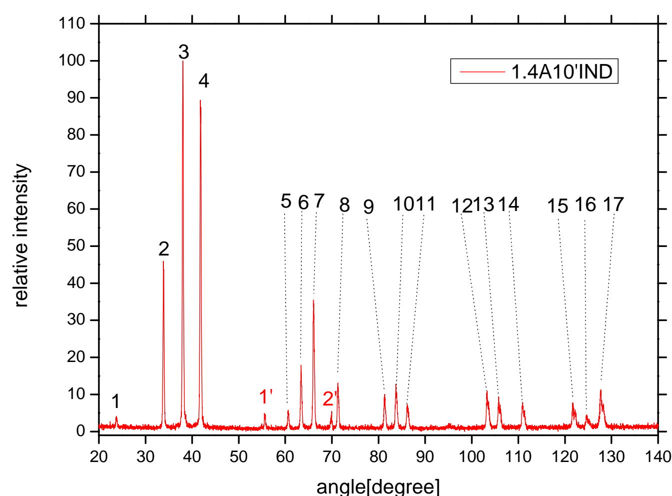

Fig. 3.52 the XRD result of Nb sputtering current 1.4A with annealing for 10 minutes

Table 3.16 the description of the peaks of 1.4A with annealing for 10 minutes

number	1	2	3	4	5	6	7	8	9	10	11	12	13	14	15	16	17
angle	23.75	33.84	37.99	41.79	60.58	63.36	66.01	71.24	81.26	83.73	86.16	103.3	105.79	110.93	121.69	124.67	127.63
plane	110	200	210	211	222	320	321	400	420	421	332	520	521	440	600	610	611
number	1'	2'															
angle	55.56	69.82															
plane	Nb200	Nb220															

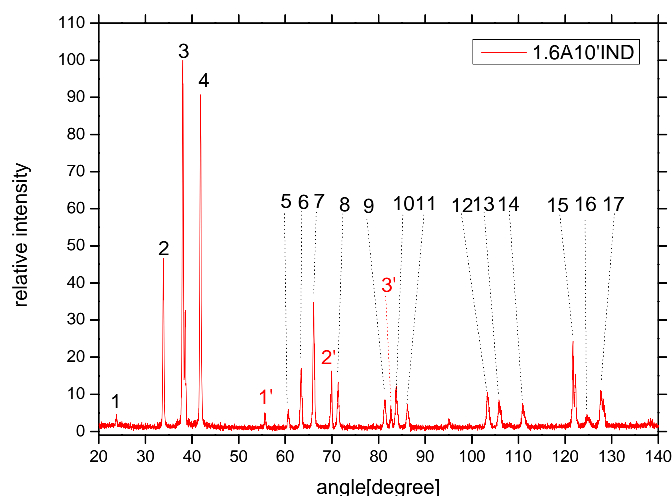

Fig. 3.53 the XRD result of Nb sputtering current 1.6A with annealing for 10 minutes

Table 3.17 the description of the peaks of 1.6A with annealing for 10 minutes

number	1	2	3	4	5	6	7	8	9	10	11	12	13	14	15	16	17
angle	23.64	33.85	37.99	41.78	60.61	63.35	66.04	71.27	81.28	83.74	86.17	103.31	105.84	110.92	121.71	124.63	127.71
plane	110	200	210	211	222	320	321	400	420	421	332	520	521	440	600	610	611
number	1'	2'	3'														
angle	55.63	69.84	82.64														
plane	Nb200	Nb211	Nb220														

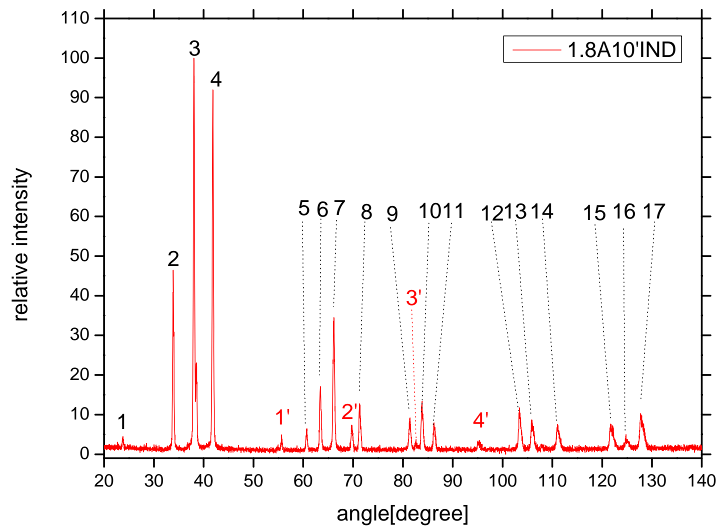

Fig. 3.54 the XRD result of Nb sputtering current 1.8A with annealing for 10 minutes

Table 3.18 the description of the peaks of 1.8A with annealing for 10 minutes

number	1	2	3	4	5	6	7	8	9	10	11	12	13	14	15	16	17
angle	23.79	33.88	38.02	41.81	60.65	63.38	66.07	71.29	81.33	83.79	86.23	103.37	105.88	110.99	121.71	124.73	127.77
plane	110	200	210	211	222	320	321	400	420	421	332	520	521	440	600	610	611
number	1'	2'	3'	4'													
angle	55.61	69.71	82.55	95.16													
plane	Nb200	Nb211	Nb220	Nb310													

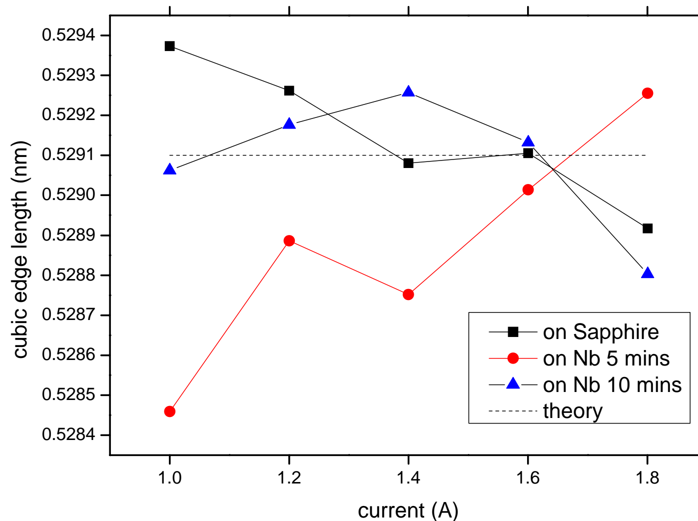

Fig.3.55 comparison of the cubic edge length between the Nb and sapphire sample

According to the XRD analysis of all of the samples of 10 minutes annealing example, there are Nb and Nb_3Sn crystal plane but not Sn crystal plane. Only the

sample with the Nb sputtering current of 1.0A has the great peak of the Nb crystal plane, but all of the peaks of all samples are smaller than that of 5 minutes annealing.

The cubic edge length of the Nb_3Sn thin film on the sapphire and Nb are calculated and shown in Fig.3.55. The cubic edge length of the thin film depositing on the sapphire decreases with the increasing of the Nb sputtering current. But the curves of the Nb sample when the annealing time is different.

3.4 Conclusion

The T_c of the Nb_3Sn multilayer deposited on the sapphire and annealed by the lamp is about 17K and the RRR of that is about 5. This result is not good enough, especially for the RRR. So we need more investigation, such as changing the proceeding gas pressure and so on.

The result of Nb_3Sn multilayer deposited on Nb and annealed by the inductor is also not good enough, but the multilayer without cover layer of Nb seems to have the better performance, in spite of the peaks of the Nb crystal plane of this kind of film are higher than the other kinds of. So the next investigation should include the changing the proceeding gas pressure and comparing the thin film between with and without the cover layer.

The reason of that multilayer deposition without the over layer is needed for further investigation is that when we deposit the thin film of Nb_3Sn on the accelerator cavity, it is impossible to use two magnetrons as shown in our experiment, and it is possible to use a post target [34] for thin film deposit, and then it is some complicated to change another target if we want to deposit the Nb cover layer.

In the conclusion, there are four jobs needed to do in future: the first job is to research the effect on the thin film of the proceeding gas pressure; the second job is to research the effect of the annealing time of the inductor; the third job is to research the effect of the Nb over layer; the fourth job is to research the deposition on the cavity.

Reference

1. A. Godeke, Nb3Sn FOR RADIO FREQUENCY CAVITIES
2. J. I. Gittleman and B. Rosenblum, Phys. Rev. Lett. 16, 734 (1966).
3. C. P. Bean and J. D. Livingston, Phys. Rev. Lett. 12, 14 (1964).
4. E. H. Brandt, Electrodynamics of superconductors exposed to high frequency fields, Presented at the international workshop on thin films and new ideas for pushing the limits of RF superconductivity, Legnaro, Italy, 2006.
5. A. Gurevich, RF breakdown in multilayer coatings: a possibility to break the Nb monopoly, Presented at the international workshop on thin films and new ideas for pushing the limits of RF superconductivity, Legnaro, Italy, 2006.
6. T. Hays, H. Padamsee, Proceeding of the 1997 workshop on RF superconductivity, 798, 1997
7. International Linear Collider Reference Design Report, volume 3, 82, August 2007
8. V. Palmieri, new materials for superconducting radiofrequency cavities, the 10th workshop on RF superconductivity, 162, 2001
9. Hartmann, Hellmuth; Ebert, Fritz; Bretschneider, Otto (1931). " Elektrolysen in Phosphatschmelzen. I. Die elektrolytische Gewinnung von α- und β-Wolfram". Zeitschrift für anorganische und allgemeine Chemie 198: 116. doi:10.1002/zaac.19311980111.
10. Kiss, A. B. (1998). Journal of Thermal Analysis and Calorimetry 54: 815. doi:10.1023/A:1010143904328.
11. Boren, B. (1933). "X-Ray Investigation of Alloys of Silicon with Chromium, Manganese, Cobalt and Nickel". Ark. Kern., Min. Geol 11A (10): 2–10.
12. Hardy, George; Hulm, John (1953). "Superconducting Silicides and Germanides". Physical Review 89: 884. doi:10.1103/PhysRev.89.884
13. Izyumov, Yurii A; Kurmaev, Z Z (1974). "Physical properties and electronic structure of superconducting compounds with theβ-tungsten structure". Soviet Physics Uspekhi 17: 356. doi:10.1070/PU1974v017n03ABEH004136.
14. Sheahen, Thomas P (1994). Introduction to high-temperature superconductivity. p. 32.
15. R. Di Leo, G. Nobile, V. Palmieri, R. Vaglio, E.C. Matacotta, E. Olzi, G. Tunisini, Weak Superconductivity, Progress on High Temperature Superconductivity, A. Barone, A. Larkin eds, World Scientific, Vol. IV, p. 275 (1987)
16. A. Nigro, G. Nobile, V. Palmieri, R. Vaglio, Adv. Cryog. Eng. 34, 813 (1988)
17. R. Di Leo, A. Nigro, G. Nobile, R. Vaglio, J. Low Temp. Phys. 78, 41 (1990)
18. M. Marino, Proceedings of the Eighth Workshop on RF Superconductivity, October 1997, Abano Terme (Padua), V. Palmieri and A. Lombardi Eds, LNLINFN (Rep) 133/98, vol.IV, p.1076
19. G. Mueller, P. Kneisel, D. Mansen, H.Piel, J.Pouryamout, R.W.Roeth, Proc. of the 5-th EPAC, London, (1985), p.2085
20. J.Nagamatsu, N.Nakagawa, T.Muranaka, Y. Zenitani, J. Akimitsu, Nature (London) 410, 63 (2001)
21. Morton E. Jones and Richard E. Marsh (1954). "The Preparation and Structure of Magnesium Boride, MgB2". Journal of the American Chemical Society 76: 1434.
22. D.C. Larbalestier et al, Nature (London) 410, 186 (2001)
23. Eisterer, M (2007). "Magnetic properties and critical currents of MgB_2". *Superconductor Science and Technology* 20: R47. doi:10.1088/0953-2048/20/12/R01.

24. Pogrebnyakov A. V., Redwing J. M., Jones J. E., Xi X. X., Xu S. Y., Li Q., VaithyanathanV. and Schlom D. G. 2003 Appl. Phys. Lett. 82 4319
25. X. X. Xi, Supercond. Sci. Technol. 22 (2009) 043001
26. Zeng X H et al 2003 Appl. Phys. Lett. 82 2097
27. Vaglio, Particle Accelerators 61, 391 (1998)
28. IavaroneM., Karapetrov G., Menzel A., Komanicky V., You H., Kwok W. K., Orgiani P., Ferrando V. and Xi X. X., 2005 Characterization of off-axis MgB2 epitaxial thin films for planar junctions Appl. Phys. Lett. 87 242506
29. C. Benvenuti, S. Calatroni, I. E. Campisi1, P. Darriulat, C. Durand2, M. Peck, R. Russo, A.-M. Valente, Proceedings of the 1997 Workshop on RF Superconductivity, (1997), 1028
30. R. Vaglio, C. Attanasio, L. Maritato, A. Ruosi, Physical Review B, 47, (1993), 15302
31. H. Hochmuth and M. Lorenz, Physical Review C, 220, (1994), 209-214
32. J. P. Charlesworth, I. Macphail and P. E. Madsen, J. Mat. Sci. 5 (1970) 580
33.. J. K. Hulm, C. K. Jones, R. A. Hein, J. W. Gibson, Journal of Low Temperature Physics, Vol. 7, (1972) 291
34. S.M. Deambrosis, G. Keppel, N. Patron, N. Pretto, V. Rampazzo, A. Rossi, R.G. Sharma, S. Stark, F. Stivanello, and V. Palmieri, Proceedings of the Eighth Workshop on RF Superconductivity, October 2007, WE203, 392